Pergamon

Int. J. Solids Structures Vol. 34, No. 25, pp. 3291–3320, 1997

0020–7683/97 $17.00 + .00

PII: S0020–7683(96)00191–6

EFFECTS OF YIELD SURFACE SHAPE AND ROUND-OFF VERTEX ON CRACK-TIP FIELDS FOR PRESSURE-SENSITIVE MATERIALS

W. J. CHANG and J. PAN
Mechanical Engineering and Applied Mechanics, The University of Michigan, Ann Arbor, Michigan, U.S.A.

(*Received* 29 *June* 1995; *in revised form* 29 *August* 1996)

Abstract—Asymptotic crack-tip fields for both power-law hardening and perfectly-plastic pressure-sensitive materials based on a modified Drucker–Prager yield criterion are obtained under plane strain conditions. The Drucker–Prager yield criterion is expressed as a linear combination of the effective stress and the mean stress. Because of the mathematical difficulty in developing the HRR-type asymptotic crack-tip fields due to the vertex of the yield surface based on the Drucker–Prager yield criterion, the vertex is rounded off and replaced by a curved yield surface which is based on a quadratic function of the effective stress and the mean stress. The HRR-type asymptotic solutions become available after rounding-off the vertex under the conditions where the asymptotic solution procedure breaks down based on the original Drucker–Prager yield criterion. The crack-tip fields for materials with large pressure sensitivity are sensitive to the ratio of the mean stress to the effective stress where the yield surface becomes quadratic. Specifically, as the stress ratio decreases, ahead of the tip the opening stress becomes larger than the radial stress, and the plastic deformation becomes concentrated to the front of the crack tip. As the stress ratio increases, the stress state ahead of the tip is shown to approach to purely hydrostatic tension, and the plastic deformation shifts backward to concentrate below and above the tip. As pressure sensitivity increases and the stress ratio decreases, the generalized effective stress contour, which can be regarded as an approximate plastic zone contour, shifts to the front of the tip. The elongated shape of approximate plastic zones for materials with large pressure sensitivity agrees with the experimental observations of the shear yielding zones near cracks in rubber-modified plastics and with the computational results for materials based on the Drucker–Prager yield criterion with large pressure sensitivity. © 1997 Elsevier Science Ltd.

1. INTRODUCTION

In the classical plasticity theory, it is generally assumed that hydrostatic pressure has no effect on material plastic deformation, and plastic dilatancy is neglected. However, for many materials such as soils, concretes, rocks and silicate glasses, pressure-sensitive yielding and plastic volumetric deformation are exhibited. Plastics also show pressure-sensitive yielding and plastic volumetric deformation (for example, see Whitney and Andrews, 1967; Sternstein and Ongchin, 1969; Rabinowtz *et al.*, 1970; Drucker, 1973; Sauer *et al.*, 1973; Spitzig and Richmond, 1979; and Carapellucci and Yee, 1986). Pressure-sensitive yielding is also observed in zirconia-containing transformation toughened ceramics (for example, see Chen and Reyes Morel, 1986; Reyes-Morel and Chen, 1988; Yu and Shetty, 1989). It is considered that the pressure-sensitive yielding occurs from basic flow mechanism in plastics and from phase transformation in phase transformation ceramics. Voids and other forms of defects can also result in macroscopic pressure sensitivity, see Gurson (1975) for porous materials with pressure-insensitive matrices and Jeong and Pan (1995) for porous materials with pressure-sensitive matrices.

Li and Pan (1990a, 1990b) studied the pressure-sensitive yielding effects on asymptotic crack-tip fields based on the Drucker–Prager yield criterion (Drucker and Prager, 1952) for power-law hardening materials and perfectly plastic materials under both plane strain and plane stress conditions. The Drucker–Prager yield criterion is expressed as a linear combination of the mean stress and the effective stress which is related to the second invariant of the stress deviator. Li and Pan (1990a, 1990b) found that the HRR-type asymptotic crack-tip fields (Hutchinson, 1968a, 1968b; Rice and Rosengren, 1968) do exist for power-law hardening materials for a range of pressure sensitivity. Li and Pan (1990a,

1990b) also presented the perfectly plastic crack-tip fields which agree well with the corresponding low hardening solutions. When the pressure sensitivity factor μ increases and approaches to a limit value for each hardening exponent, the stress state ahead of the crack tip approaches to purely hydrostatic tension. Beyond the limit value of μ they could not find any HRR-type asymptotic solution using the Runge–Kutta method for numerical integration and the shooting method for satisfying the boundary conditions.

Pan and Chen (1991) then used a finite element method for deformation plasticity power-law hardening materials to investigate the asymptotic crack-tip fields under plane strain and small-scale yielding conditions. Their results showed that for μ larger than the limit value for each hardening exponent, the HRR-type crack-tip field does exist and the stress state ahead of the tip stays in purely hydrostatic tension for a range of μ. When μ becomes larger than a value near $\sqrt{3}/2$, the HRR-type crack-tip field breaks down and the near-tip field becomes oscillatory. Dong and Pan (1991) investigated the crack-tip fields by finite element methods for elastic–plastic pressure-sensitive dilatant materials under plane strain and small-scale yielding conditions. Their results also indicated that the HRR-type asymptotic crack-tip fields exist beyond the limit value of the pressure sensitivity factor for each hardening exponent for power-law hardening materials, and that elastic sectors of finite stresses exist and border the crack faces for elastic perfectly plastic materials, in contrast to the fully yielded solutions based on the slip-line theory proposed by Li and Pan (1990a). Their perfectly plastic finite element solutions also indicated that when μ is larger than $\sqrt{3}/2$, no asymptotic solutions can be found. Due to the discretization of the finite element method, the computational results obtained by Pan and Chen (1991) and Dong and Pan (1991) can be regarded as the results based on the Drucker–Prager yield criterion with a round-off vertex. The curvature of the round-off vertex is related to the size of the finite elements directly ahead of the tip.

The yield criteria for plastics and phase transformation ceramics appear to be linear in terms of the effective stress and the mean stress, from the stress state with very large negative mean stress to the uniaxial tensile stress state according to the experimental evidences (Drucker, 1973; Chen and Reyes Morel, 1986; Reyes-Morel and Chen, 1988). However, the Drucker–Prager yield criterion at large mean stress near the state of purely hydrostatic tension has not been validated due to experimental difficulties. From the material viewpoint, we expect that large tensile stresses tend to enlarge the existing defects such as voids or microcracks in materials and yielding should occur earlier than that predicted by the Drucker–Prager yield criterion. Also invoking the convexity of the yield surface should result in the same conclusion. Of course, a yield criterion for voided materials proposed by Gurson (1975) can shed some light on the material yielding behavior at large hydrostatic tension. In fact, Gurson's yield criterion and its modified form (Tvergaard, 1980, 1981) have been used extensively to study the stress and deformation field near crack tips in ductile materials, see Aoki *et al.* (1984), Aravas and McMeeking (1985) and Needleman and Tvergaard (1987).

A recent investigation of the deformation fields near crack tips in rubber-modified plastics by Pearson and Yee (1991) indicated that the intense plastic straining appears to be concentrated ahead of the tip. Also, Yu and Shetty (1989) showed that the phase transformation zones near cracks in zirconia ceramics appear to be concentrated ahead of the tip. A finite element analysis by Jeong and Pan (1996) based on a generalized Gurson's yield criterion (Jeong and Pan, 1995) for porous materials with pressure-sensitive matrices showed an elongated intense straining zone ahead of the crack tip, which is in good agreement with the experimental observation of Pearson and Yee (1991). The finite element analyses of Pan and Chen (1991), Dong and Pan (1991) and Kim and Pan (1994) indicated that plastic deformation does become concentrated ahead of the tip for materials based on the Drucker–Prager yield criterion with large pressure sensitivity. A common feature of the deformation patterns near cracks in plastics and phase transformation ceramics is elongated intense straining zone and phase transformation zone ahead of the tips. The main reason for causing the common deformation pattern can be rationalized as the large pressure sensitivity of yielding for materials near the crack tips. For phase transformation ceramics, the large pressure sensitivity comes from the intrinsic nature of phase transformation. For

toughened plastics, the large pressure sensitivity comes from the extensive cavitation near the tips. In order to seek a relatively simple analysis to substantiate this rationalization, HRR-type asymptotic analyses of crack-tip fields have been carried out (Li and Pan, 1990a, 1990b). However, due to the mathematical difficulty associated with the vertex of the Drucker–Prager's yield surface for materials with large pressure sensitivity, no simple theoretical verification of the computational results for phase transformation ceramics and toughened plastics has been obtained. Therefore, we here modify the Drucker–Prager yield criterion and intend to understand the crack-tip fields for materials with large pressure sensitivity.

Specifically, when the ratio of the mean stress to the effective stress becomes large, to avoid the existence of the vertex on the yield surface based on the Drucker–Prager yield criterion, we approximate the yield criterion based on a quadratic function of the mean stress and the effective stress following the arguments of the existence of defects and the convexity of the yield surface. In this way we can study the effects of the yield surface shape on the asymptotic crack-tip fields under plane strain conditions based on this modified Drucker–Prager yield criterion. According to the asymptotic crack-tip solutions for low hardening materials, we are then able to assemble perfectly-plastic asymptotic solutions based on the modified Drucker–Prager yield criterion as well as a parabolic type of yield criterion. The implications of the geometric shape of the yield surface to the crack-tip fields are presented and discussed.

2. CONSTITUTIVE RELATIONS

Based on the experimental results of polymers and phase transformation ceramics, the yielding of these materials follows the Drucker–Prager yield criterion from the stress state with very large negative mean stress to the uniaxial tensile stress state. The Drucker–Prager yield criterion can be written as a linear combination of the mean stress σ_m $(=\sigma_{kk}/3)$ and the effective tensile stress σ_e $(=(3s_{ij}s_{ij}/2)^{1/2}$ where $s_{ij}=\sigma_{ij}-\sigma_m\delta_{ij})$:

$$\psi(\sigma_{ij}) = \sigma_e + \sqrt{3}\mu\sigma_m = \sigma_{ge}. \tag{1}$$

In eqn (1), μ is a material constant and represents the pressure sensitivity of yielding, σ_{ge} represents the generalized effective tensile stress, and $\psi(\sigma_{ij})$ represents the yield surface in the stress space. For steels, the values of μ are quite small in the range from 0.014 to 0.064 (Spitzig *et al.*, 1975, 1976). For polymers, the values of μ are in the range from 0.1 to 0.25 (Kinloch and Young, 1983). For phase transformation ceramics, Chen (1991) reported that μ is 0.55 for Mg-PSZ and 0.77 for Ce-TZP. For Ce-TZP, μ can be as high as 0.93 (Yu and Shetty, 1989). The yield criterion can be plotted as a straight line inclined to the σ_e axis in the σ_m–σ_e plane as shown in Fig. 1. The value of the slope of the straight line is $\sqrt{3}\mu$ as shown. When μ becomes zero, the yield contour becomes a straight line parallel to the σ_m axis and the Mises yield criterion is recovered.

To specify the initial yield surface, we set $\sigma_{ge}=\sigma_0$. Then σ_0 and μ can be determined from uniaxial tensile and compressive tests as

$$\mu = \sqrt{3}\frac{\sigma_c-\sigma_t}{\sigma_c+\sigma_t} \quad \text{and} \quad \sigma_0 = \frac{2\sigma_c\sigma_t}{\sigma_c+\sigma_t}, \tag{2}$$

where σ_c is the initial compressive yield stress and σ_t is the initial tensile yield stress. The yield surface of the Drucker–Prager yield criterion in the principal stress space has the shape of a cone and exhibits a vertex at the cone tip. The vertex on the yield surface results in a singularity in the constitutive law when the associated flow rule is employed. In order to avoid the singularity in the constitutive relation based on the Drucker–Prager yield criterion, and motivated by the geometric shape of the yield surface for steels (Gurson, 1975, 1977) and plastics with voids (Jeong and Pan, 1995), we modify the linear yield contour near the σ_m axis by a quadratic yield contour as shown in Fig. 1. The quadratic

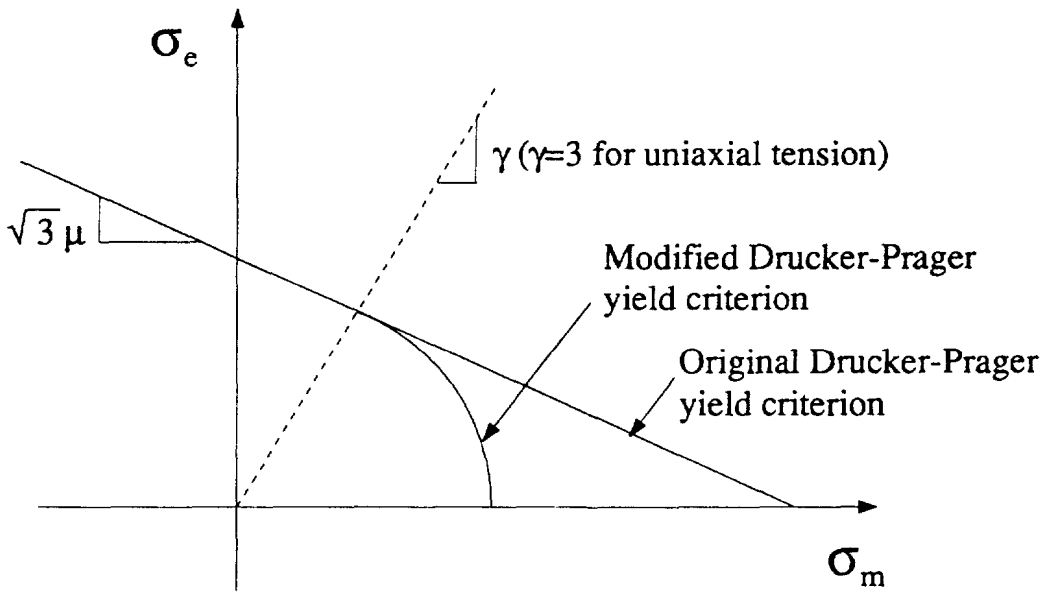

Fig. 1. The Drucker–Prager yield criterion and a modified Drucker–Prager yield criterion illustrated in the σ_m–σ_e plane.

yield contour and the linear yield contour defined by eqn (1) are demarcated by a specific ratio σ_e/σ_m. It should be noted that the inclusion of a quadratic portion of the yield surface to replace the vertex is to facilitate the finding of the HRR-type crack-tip fields and to understand qualitatively the effects of the round-off vertex on the crack-tip stress and strain fields.

We denote this ratio σ_e/σ_m as γ. Then we can express our modified Drucker–Prager yield criterion as

$$\psi(\sigma_{ij}) = \sigma_e + \sqrt{3}\mu\sigma_m = \sigma_{ge} \quad \text{for} \quad \sigma_m/\sigma_e \leqslant 1/\gamma \tag{3}$$

$$\psi(\sigma_{ij}) = (A\sigma_e^2 + B\sigma_m^2)^{1/2} = \sigma_{ge} \quad \text{for} \quad \sigma_m/\sigma_e > 1/\gamma \tag{4}$$

where

$$A = \frac{\gamma + \sqrt{3}\mu}{\gamma} \quad \text{and} \quad B = \sqrt{3}\mu(\gamma + \sqrt{3}\mu). \tag{5}$$

The constants A and B are determined from the continuity conditions of the yield contours and their outward normals at $\sigma_e/\sigma_m = \gamma$. As μ approaches 0, the Mises yield criterion is recovered from our modified Drucker–Prager yield criterion for any ratio γ.

It should be noted that eqn (3) appears to be linear and eqn (4) quadratic in terms of σ_e and σ_m. Although σ_e is related to a quadratic function of σ_{ij}, we call eqn (3) linear and eqn (4) quadratic for simplicity. Also, $\sigma_e/\sigma_m = 3$ represents uniaxial tensile loading. When we take $\gamma = 3$, the material will follow the Drucker–Prager yield criterion from all compressive loading conditions to uniaxial tensile loading condition. If a very small number is assigned to γ, the yield criterion will be almost the same as the original Drucker–Prager yield criterion except a very small quadratic region close to the state of purely hydrostatic tension. Furthermore, the outward normal to the modified Drucker–Prager yield criterion at $\sigma_e = 0$ is parallel to the σ_m axis due to the addition of the quadratic region. When the normality rule is employed, a purely dilatational plastic strain rate corresponds to a purely hydrostatic tension. This satisfies the symmetry condition for isotropic materials.

Based on the modified Drucker–Prager yield criterion in eqns (3) and (4), the curvature of a constant σ_{ge} contour in the σ_m–σ_e plane is 0 in the linear region but varies in the quadratic region. Note that the quadratic yield function in eqn (4) represents an ellipse in

the σ_m–σ_e plane with the major axis in the σ_m direction when $A > B$ and with the major axis in the σ_e direction when $A < B$. The curvature of an elliptical contour increases monotonically from the intersection with the minor axis to the intersection with the major axis. Therefore the curvature of the quadratic contour increases monotonically from $\sigma_e/\sigma_m = \gamma$ to $\sigma_e/\sigma_m = 0$ when $A > B$, and decreases monotonically from $\sigma_e/\sigma_m = \gamma$ to $\sigma_e/\sigma_m = 0$ when $A < B$. When A is equal to B, the quadratic yield contour becomes circular and the curvature remains constant in the quadratic region. The curvature κ of the quadratic yield contour at the border of the linear and the quadratic regions, where $\sigma_e/\sigma_m = \gamma$, can be represented as

$$\kappa = \frac{|\mathrm{d}^2\sigma_e/\mathrm{d}\sigma_m^2|}{(1+(\mathrm{d}\sigma_e/\mathrm{d}\sigma_m)^2)^{3/2}} = \frac{1}{\sigma_{ge}} \frac{\sqrt{3}\mu(\gamma+\sqrt{3}\mu)^2}{\gamma(1+3\mu^2)^{3/2}} \tag{6}$$

where all the derivatives in eqn (6) are calculated based on the quadratic yield function in eqn (4) with σ_{ge} = constant. It should be noted that the curvature κ of the quadratic yield contour at $\sigma_e/\sigma_m = \gamma$ is finite when $\gamma \neq 0$. Therefore, when the yield contour changes from linear to quadratic at $\sigma_e/\sigma_m = \gamma$, the curvature has a jump from 0 to a finite value. The normalized curvatures $\kappa\sigma_{ge}$ of the quadratic yield contour at $\sigma_e/\sigma_m = \gamma$ as functions of γ are shown in Fig. 2 for several values of μ. For a given μ, $\kappa\sigma_{ge}$ decreases and then increases rapidly as γ decreases. Therefore a local minimum of $\kappa\sigma_{ge}$ occurs. According to eqn (6), the local minimum occurs at $\gamma = \sqrt{3}\mu$. According to eqn (6), as γ decreases to 0, $\kappa\sigma_{ge}$ approaches to infinity and the original Drucker–Prager yield criterion is recovered with an infinite curvature at $\sigma_e = 0$.

The deformation plasticity constitutive relations for power-law hardening materials based on the Drucker–Prager yield criterion has been elaborated in Li and Pan (1990a). The use of deformation plasticity for asymptotic analyses of crack-tip fields for incremental plasticity materials was discussed in Hutchinson (1968a). We follow the procedure of Li

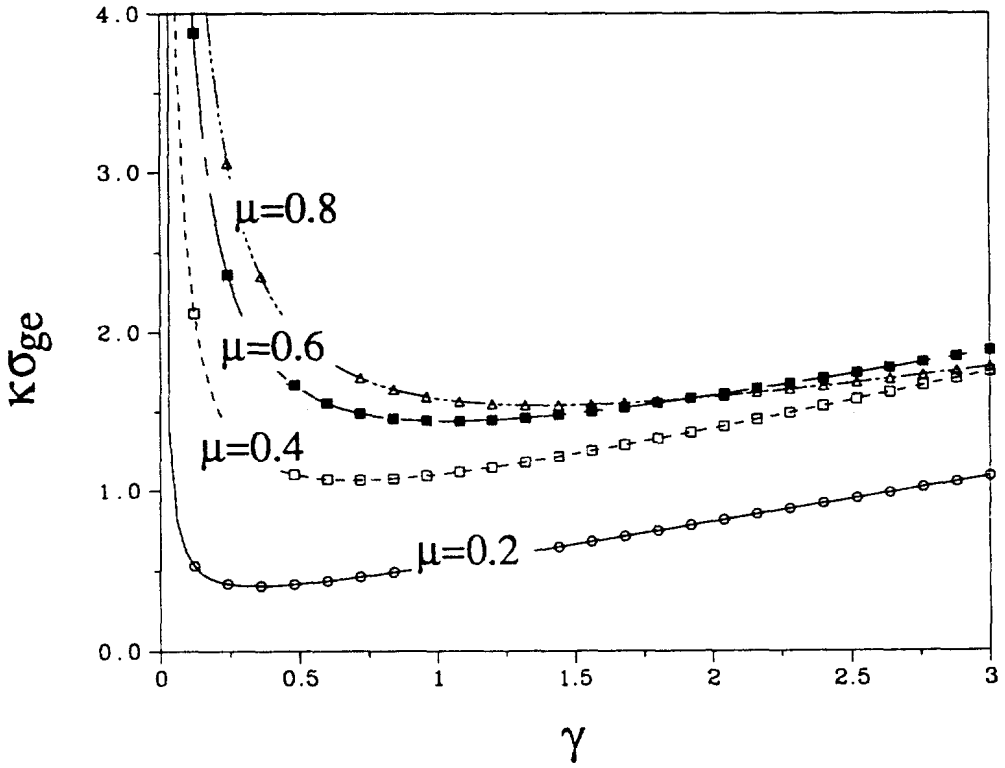

Fig. 2. The normalized curvature of the quadratic yield contour at the border of the linear region and quadratic region jumps from 0 on the linear side to the value shown in the figure on the quadratic side as a function of γ for $\mu = 0.2$, 0.4, 0.6, and 0.8.

and Pan (1990a) to develop the constitutive relations based on the quadratic part of the yield criterion. We assume a power-law stress–strain relation

$$\frac{\varepsilon_{ge}^p}{\varepsilon_0} = \alpha \left(\frac{\sigma_{ge}}{\sigma_0}\right)^n, \tag{7}$$

where ε_0 is the reference strain, σ_0 is the reference stress, α is a material constant, n is the hardening exponent, and ε_{ge}^p is the generalized effective plastic strain. Here the differential of ε_{ge}^p is defined as the work conjugate of σ_{ge}. When the normality flow rule is assumed, the deformation plasticity constitutive relations for the stresses and plastic strains in the linear and quadratic regions can be described as

$$\frac{\varepsilon_{ij}^p}{\varepsilon_0} = \alpha \left(\frac{\sigma_{ge}}{\sigma_0}\right)^n \left(\frac{3s_{ij}}{2\sigma_e} + \frac{\mu}{\sqrt{3}}\delta_{ij}\right) \quad \text{for} \quad \sigma_m/\sigma_e \leqslant 1/\gamma \tag{8}$$

$$\frac{\varepsilon_{ij}^p}{\varepsilon_0} = \alpha \left(\frac{\sigma_{ge}}{\sigma_0}\right)^{n-1} \left(\frac{3}{2}A\frac{s_{ij}}{\sigma_0} + \frac{1}{3}B\frac{\sigma_m}{\sigma_0}\delta_{ij}\right) \quad \text{for} \quad \sigma_m/\sigma_e > 1/\gamma, \tag{9}$$

where A and B are functions of μ and γ as described in eqn (5).

Note that when $\mu = 0$, the J_2 deformation plasticity is recovered from both eqns (8) and (9). One can easily examine that the constitutive relations in eqns (8) and (9) are equivalent when $\sigma_e/\sigma_m = \gamma$ so that there will be no conflict on the constitutive behavior when the material undergoes the transition from the linear region to the quadratic region and vice versa. The generalized effective plastic strains ε_{ge}^p has the form of

$$\varepsilon_{ge}^p = \left(\tfrac{2}{3}e_{ij}^p e_{ij}^p\right)^{1/2} \quad \text{for} \quad \sigma_m/\sigma_e \leqslant 1/\gamma \tag{10}$$

$$\varepsilon_{ge}^p = \left(\frac{2}{3A}e_{ij}^p e_{ij}^p + \frac{1}{B}\varepsilon_{ij}^p e_{ij}^p\right)^{1/2} \quad \text{for} \quad \sigma_m/\sigma_e > 1/\gamma, \tag{11}$$

where e_{ij}^p ($= \varepsilon_{ij}^p - \varepsilon_{kk}^p/3$) are the deviatoric plastic strains.

When the elastic strains are negligible compared to the plastic strains and the plane strain condition $\varepsilon_{33} = 0$ is assumed, we can derive the constitutive equations in terms of the in-plane stresses (σ_{11}, σ_{22} and σ_{12}) and in-plane strains ($\varepsilon_{11}, \varepsilon_{22}$ and ε_{12}). In the linear region where $\sigma_m/\sigma_e \leqslant 1/\gamma$, we have (Li and Pan, 1990a)

$$\frac{\varepsilon_{11}}{\varepsilon_0} = \frac{3}{2}\alpha \left(\frac{\sigma_{ge}}{\sigma_0}\right)^n \left[\frac{\sigma_{11}-\sigma_{22}}{2\sigma_e} + \frac{\mu}{\sqrt{3}}\right]$$

$$\frac{\varepsilon_{22}}{\varepsilon_0} = \frac{3}{2}\alpha \left(\frac{\sigma_{ge}}{\sigma_0}\right)^n \left[\frac{\sigma_{22}-\sigma_{11}}{2\sigma_e} + \frac{\mu}{\sqrt{3}}\right]$$

$$\frac{\varepsilon_{12}}{\varepsilon_0} = \frac{3}{2}\alpha \left(\frac{\sigma_{ge}}{\sigma_0}\right)^n \left[\frac{\sigma_{12}}{\sigma_e}\right]$$

where

$$\sigma_{ge} = \left(1-\frac{\mu^2}{3}\right)^{1/2} \left[\frac{3}{4}(\sigma_{11}-\sigma_{22})^2 + 3\sigma_{12}^2\right]^{1/2} + \frac{\sqrt{3}\mu}{2}(\sigma_{11}+\sigma_{22}) \tag{12}$$

and

$$\sigma_e = \left(1-\frac{\mu^2}{3}\right)^{-1/2}\left[\frac{3}{4}(\sigma_{11}-\sigma_{22})^2+3\sigma_{12}^2\right]^{1/2}. \tag{13}$$

The other stress components of interest in the linear region are the out-of-plane stress σ_{33} and the mean stress σ_m. They can be represented as

$$\sigma_{33} = \frac{\sigma_{11}+\sigma_{22}}{2} - \frac{\mu}{\sqrt{3}}\sigma_e \tag{14}$$

$$\sigma_m = \frac{\sigma_{11}+\sigma_{22}}{2} - \frac{\mu}{3\sqrt{3}}\sigma_e. \tag{15}$$

In the quadratic region where $\sigma_m/\sigma_e > 1/\gamma$, we have

$$\frac{\varepsilon_{11}}{\varepsilon_0} = \frac{3}{2}\alpha\left(\frac{\sigma_{ge}}{\sigma_0}\right)^{n-1}\frac{1}{\sigma_0}\left\{A\left[\frac{9A+4B}{18A+2B}\sigma_{11}-\frac{9A-2B}{18A+2B}\sigma_{22}\right]\right\}$$

$$\frac{\varepsilon_{22}}{\varepsilon_0} = \frac{3}{2}\alpha\left(\frac{\sigma_{ge}}{\sigma_0}\right)^{n-1}\frac{1}{\sigma_0}\left\{A\left[\frac{9A+4B}{18A+2B}\sigma_{22}-\frac{9A-2B}{18A+2B}\sigma_{11}\right]\right\}$$

$$\frac{\varepsilon_{12}}{\varepsilon_0} = \frac{3}{2}\alpha\left(\frac{\sigma_{ge}}{\sigma_0}\right)^{n-1}\frac{1}{\sigma_0}\{A\sigma_{12}\}$$

where

$$\sigma_{ge} = \left[\frac{3}{4}A\left(\frac{9A+4B}{9A+B}\right)(\sigma_{11}^2+\sigma_{22}^2)-\frac{3}{2}A\left(\frac{9A-2B}{9A+B}\right)\sigma_{11}\sigma_{22}+3A\sigma_{12}^2\right]^{1/2}. \tag{16}$$

The other stress components of interest in the quadratic region are

$$\sigma_e = [\alpha_1(\sigma_{11}^2+\sigma_{22}^2)-\sigma_2\sigma_{11}\sigma_{22}+3\sigma_{12}^2]^{1/2} \tag{17}$$

$$\sigma_{33} = \frac{9A-2B}{18A+2B}(\sigma_{11}+\sigma_{22}) \tag{18}$$

$$\sigma_m = \frac{9A}{18A+2B}(\sigma_{11}+\sigma_{22}) \tag{19}$$

where

$$\alpha_1 = \frac{3}{4}\frac{81A^2+18AB+4B^2}{(9A+B)^2} \tag{20}$$

and

$$\alpha_2 = -\frac{3}{2}\frac{81A^2+18AB-2B^2}{(9A+B)^2}. \tag{21}$$

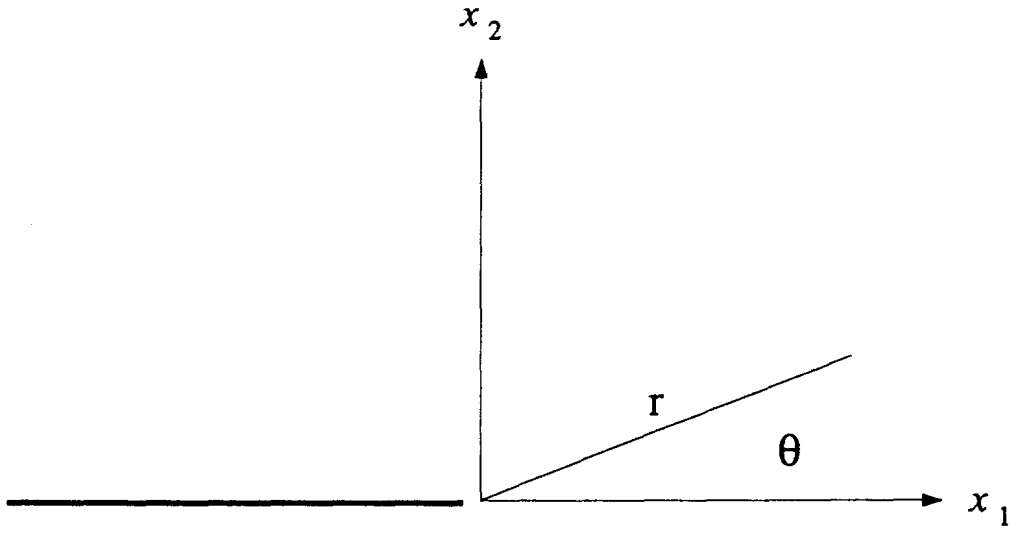

Fig. 3. The coordinate convention of a planar crack problem.

3. DOMINANT SINGULARITY ANALYSIS

We consider a planar crack problem as illustrated in Fig. 3, where the Cartesian coordinates (x_1, x_2) and the associated polar coordinates (r, θ) are centered at the crack tip and the x_3 axis lies perpendicular to the x_1–x_2 plane. The dominant asymptotic crack-tip fields have been obtained for power-law hardening Mises materials by Hutchinson (1968a, 1968b) and Rice and Rosengren (1968). For power-law hardening Drucker–Prager materials, the asymptotic crack-tip fields for a limited range of μ have been obtained by Li and Pan (1990a, b). In the same way, the dominant asymptotic crack-tip stress, strain and displacement fields for pressure-sensitive materials based on the modified Drucker–Prager yield criterion can be written as

$$\sigma_{ij} = \sigma_0 \left[\frac{J}{\alpha\sigma_0\varepsilon_0 I(n,\mu)r}\right]^{1/n+1} \tilde{\sigma}_{ij}(\theta; n, \mu, \gamma)$$

$$\varepsilon_{ij} = \alpha\varepsilon_0 \left[\frac{J}{\alpha\sigma_0\varepsilon_0 I(n,\mu)r}\right]^{n/n+1} \tilde{\varepsilon}_{ij}(\theta; n, \mu, \gamma)$$

$$u_i = \alpha\varepsilon_0 r \left[\frac{J}{\alpha\sigma_0\varepsilon_0 I(n,\mu)r}\right]^{n/n+1} \tilde{u}_i(\theta; n, \mu, \gamma) \tag{22}$$

where J is the J-integral given by Rice (1968):

$$J = \int_\Gamma \left[W v_1 - \sigma_{ij} v_j \frac{\partial u_i}{\partial x_1}\right] \mathrm{d}s. \tag{23}$$

In eqn (23), Γ represents an arbitrary contour from the lower crack face to the upper crack face in a counterclockwise sense, W represents the strain energy density function of the deformation plasticity materials, and v_j is the jth component of the outward normal unit vector $\boldsymbol{v}$ to Γ. Here, J represents the singularity amplitude of the crack-tip field. The dimensionless constant I can be represented as

$$I = \int_{-\pi}^{\pi} \left[\frac{n}{n+1} \tilde{\sigma}_{ge}^{n+1} \cos\theta - \left[\sin\theta(\tilde{\sigma}_{rr}(\tilde{u}_\theta - \tilde{u}_r) - \tilde{\sigma}_{r\theta}(\tilde{u}_r + \tilde{u}_\theta)) + \frac{\cos\theta}{n+1}(\tilde{\sigma}_{rr}\tilde{u}_r + \tilde{\sigma}_{r\theta}\tilde{u}_\theta)\right]\right] \mathrm{d}\theta \tag{24}$$

and $\tilde{\sigma}_{ij}$, $\tilde{\varepsilon}_{ij}$, and $\tilde{u}_i$ are the dimensionless stress, strain, and displacement functions.

We follow the solution procedure used by Hutchinson (1968a, 1968b) and Shih (1973) to obtain the asymptotic crack-tip fields based on the modified Drucker–Prager yield criterion. The procedure is briefly discussed in the following. An Airy stress function of separable form in r and θ is introduced to satisfy the equilibrium equations

$$\phi = Kr^s\tilde{\phi}(\theta; n, \mu, \gamma), \tag{25}$$

where $s = (2n+1)/(n+1)$ is the eigenvalue obtained by the argument of the path independence of the J-integral (Rice and Rosengren, 1968). The strain components are expressed in terms of the stress function through the plastic stress–strain relations, and then are inserted into the compatibility equation to arrive at a fourth-order non-linear ordinary differential equation with θ as the independent variable. The traction-free conditions on the crack faces provide the necessary boundary conditions for the differential equation. A shooting method based on a combined fourth-fifth order Runge–Kutta scheme with error and step-size control is employed to generate solutions.

For mode I loading, the range of θ for integration is set from 0° to 180° by taking advantage of the symmetry conditions at 0°. In this angular span, there may be two different types of sectors bordering each other: one is based on the linear part of the yield criterion and the other is based on the quadratic part of the yield criterion. Along the border of these two types of sectors, u_r, u_θ, $\sigma_{r\theta}$, and $\sigma_{\theta\theta}$ must be continuous and consequently $\tilde{u}_r$, $\tilde{u}_\theta$, $\tilde{\sigma}_{r\theta}$, and $\tilde{\sigma}_{\theta\theta}$ must be continuous. We can express these normalized functions as

$$\tilde{\sigma}_{r\theta}(\theta) = (1-s)\tilde{\phi}^{\cdot} \tag{26}$$

$$\tilde{\sigma}_{\theta\theta}(\theta) = s(s-1)\tilde{\phi} \tag{27}$$

$$\tilde{u}_r(\theta) = (n+1)\tilde{\varepsilon}_{rr} \tag{28}$$

$$\tilde{u}_\theta(\theta) = -\frac{n+1}{n}(2\tilde{\varepsilon}_{r\theta} - \tilde{u}_r), \tag{29}$$

where $(\,)^{\cdot} \equiv \partial/\partial\theta$. In eqns (28) and (29), $\tilde{\varepsilon}_{rr}$ and $\tilde{\varepsilon}_{r\theta}$ can be expressed as

$$\tilde{\varepsilon}_{rr} = \tilde{\varepsilon}_{rr}(\tilde{\phi}, \tilde{\phi}^{\cdot}, \tilde{\phi}^{\cdot\cdot}) \tag{30}$$

$$\tilde{\varepsilon}_{r\theta} = \tilde{\varepsilon}_{r\theta}(\tilde{\phi}, \tilde{\phi}^{\cdot}, \tilde{\phi}^{\cdot\cdot}). \tag{31}$$

From eqns (26), (27), (28), and (30), it is clear that $\tilde{\phi}$, $\tilde{\phi}^{\cdot}$, and $\tilde{\phi}^{\cdot\cdot}$ have to be continuous along the border. Equations (28), (29), (30), and (31) determine the jump of $\tilde{\phi}^{\cdot\cdot\cdot}$ across the border in order to have a continuous $\tilde{u}_\theta$. Note that the continuity conditions of $\tilde{\sigma}_{r\theta}$, $\tilde{\sigma}_{\theta\theta}$, and $\tilde{u}_r$ (see eqns (26), (27), and (28) with (30)) also imply the continuity of $\tilde{\sigma}_{rr}(\tilde{\phi}, \tilde{\phi}^{\cdot}, \tilde{\phi}^{\cdot\cdot})$. Thus the asymptotic solutions for power-law hardening materials shown later reveal no discontinuity of $\tilde{\sigma}_{rr}$ across the border between a linear and a quadratic sector.

The crack tip opening displacement δ_t is defined as the opening displacement between the intercepts of the two 45° lines drawn back from the crack tip with the deformed crack profile (Shih, 1981). The relation between J and δ_t has been investigated for Mises materials by Shih (1981). In the same way, we express the crack tip opening displacement δ_t as

$$\delta_t = (\alpha\varepsilon_0)^{1/n}\left(\frac{J}{\sigma_0}\right)\frac{(\tilde{u}_1+\tilde{u}_2)^{1/n}\cdot 2\tilde{u}_2}{I} \tag{32}$$

where $\tilde{u}_1 = -\tilde{u}_r(\theta=\pi)$ and $\tilde{u}_2 = -\tilde{u}_\theta(\theta=\pi)$. The length scale of δ_t in terms of J/σ_0 gives the approximate size where the effects of finite deformation should be taken into account

Table 1. The numerical values of $\gamma_{cr}(n, \mu)$ for the modified Drucker–Prager yield criterion ("—" indicates that the hardening solution is not available by the shooting method for the original Drucker–Prager yield criterion)

μ	0	0.1	0.2	0.3	0.4	0.6	0.8	$\sqrt{3}/2$
$n = 3$	0.1427	—	—	—	—	—	—	—
$n = 10$	0.3170	0.2250	0.1362	0.0461	—	—	—	—
$n = 25$	0.3708	0.2878	0.2102	0.1371	0.0674	—	—	—
$n = 50$	0.3913	0.3116	0.2376	0.1686	0.1042	—	—	—
$n = \infty$	0.4182	0.3434	0.2747	0.2116	0.1537	0.0556	0.0013	0

(McMeeking, 1977). We can rewrite eqn (32) as

$$\delta_t = (\alpha\varepsilon_0)^{1/n}\beta\left(\frac{J}{\sigma_0}\right) \tag{33}$$

where

$$\beta = \frac{(\tilde{u}_1 + \tilde{u}_2)^{1/n} \cdot 2\tilde{u}_2}{I}. \tag{34}$$

The normalized coordinates, x_1 and x_2, by δ_t for the deformed crack tip profile can be expressed as

$$\frac{x_1}{\delta_t} = -\left(\frac{r}{\delta_t}\right) + \left(\frac{r}{\delta_t}\right)^{1/n+1} \frac{\tilde{u}_1}{[(\tilde{u}_1 + \tilde{u}_2)^{1/n} \cdot 2\tilde{u}_2]^{n/n+1}} \tag{35}$$

$$\frac{x_2}{\delta_t} = \left(\frac{r}{\delta_t}\right)^{1/n+1} \frac{\tilde{u}_2}{[(\tilde{u}_1 + \tilde{u}_2)^{1/n} \cdot 2\tilde{u}_2]^{n/n+1}}. \tag{36}$$

4. CRACK-TIP FIELDS FOR POWER-LAW HARDENING MATERIALS

Mode I crack-tip fields under plane strain conditions are investigated in this paper. Our numerical results show that the HRR-type crack-tip fields based on the modified Drucker–Prager yield criterion can be obtained for $\mu < \sqrt{3}/2$ (≈ 0.866). The asymptotic crack-tip solutions are very sensitive to the exact geometric shape of the yield criterion in terms of the value of γ. Various values of γ have been selected to examine the effects of the quadratic part of the yield criterion on the crack-tip fields and to extrapolate to the crack-tip fields based on the original Drucker–Prager yield criterion with a vertex on the yield surface.

In general, for a given set of n and μ there exists a critical value of γ below which the crack-tip solutions remain the same as those given by Li and Pan (1990a). These solutions from $\theta = 0°$ to $180°$ are completely based on the linear part of the yield criterion. This critical value of γ, denoted by γ_{cr}, is essentially the minimum value of σ_e/σ_m of the solutions given by Li and Pan (1990a) for the given n and μ. In other words, if we select a modified Drucker–Prager yield criterion with γ less than γ_{cr}, then the development of the solution will not depend upon the quadratic part of the yield criterion. The values of γ_{cr} for various μ's and n's are listed in Table 1. Note that the symbol "—" in Table 1 indicates that the solution is not available by the shooting method based on the original Drucker–Prager yield criterion. In general the values of γ_{cr} are quite small for both power-law hardening and perfectly plastic materials ($n = \infty$). Note that the $1/\gamma_{cr}$ represents the ratio σ_m/σ_e ahead of the tip for materials based on the original Drucker–Prager yield criterion. For $\mu = 0$, $1/\gamma_{cr}$ decreases as the hardening exponent n increases. This indicates that the triaxality ahead of the crack tip actually decreases as n increases for Mises materials. For high hardening materials ($n = 3$), a quadratic part of the yield criterion must be introduced for

the existence of the HRR-type solutions for materials with moderately large μ, as shown by these "—" symbols in Table 1. As n increases, the requirement for incorporation of a quadratic part of the yield criterion for the existence of the HRR-type solutions actually relaxes.

For perfectly plastic materials, asymptotic solutions can always be found as long as $\mu \leqslant \sqrt{3}/2$, and the values of γ_{cr} decrease as μ increases. For perfectly plastic materials, when μ becomes large, γ_{cr} becomes very small. This implies that for perfectly plastic materials, as long as there is a curved part of the yield surface near the vertex, the curved part of the yield surface can definitely affect the asymptotic solutions. This also indicates that for low hardening and perfectly plastic materials with large pressure sensitivity the exact shape of the yield surface at large hydrostatic tension, which is difficult to obtain experimentally, is a vital information to understand the stress and deformation fields ahead of the tip. When the HRR-type solutions for hardening materials are available at the value of γ larger than γ_{cr}, an angular span based on the quadratic part of the yield criterion appears in front of the crack tip to cast the influence of the quadratic part of the yield surface on the crack-tip fields.

Figure 4 shows the normalized stress, strain and displacement fields as functions of θ for power-law hardening materials based on the modified Drucker–Prager yield criterion with $n = 10$, $\gamma = 3$, and $\mu = 0$, 0.4, and 0.8. As mentioned earlier, $\gamma = 3$ indicates that the uniaxial tensile state is used to demarcate the linear and quadratic parts of the yield criterion. The results show the effects of the curved yield surface on the crack-tip stress and deformation fields. In these figures, we mark "Linear Region" for regions based on the linear part of the yield criterion and "Quadratic Region" for regions based on the quadratic part of the yield criterion. For $\mu = 0$, we mark "Quadratic/Linear" because the Mises yield criterion is recovered for both the linear part and quadratic part of the yield criterion, as discussed earlier.

As shown in Fig. 4(a), the stress and strain solutions for Mises materials are recovered for $\mu = 0$. Also shown in Fig. 4(a), the opening stress $\tilde{\sigma}_{\theta\theta}$ ahead of the crack tip becomes significantly larger than the other components as μ increases. For $\mu = 0.4$ and 0.8, a quadratic region appears ahead of the tip and a rapid variation on $\tilde{\sigma}_{rr}$ can be seen near $\theta = 180°$. The quadratic region is bordered at the angle where the discontinuity of the slope of $\tilde{\sigma}_{rr}$ occurs. As n increases, the angular span of the quadratic region decreases. The discontinuity of the slope of $\tilde{\sigma}_{rr}$ becomes more substantial when n and/or μ becomes large. Figure 4(b) shows that as μ increases, the plastic deformation shifts to the front of the tip. Figure 4(c) shows the normalized displacement fields as functions of θ. It should be noted that the displacements are continuous at the borders between the linear and quadratic regions. It should also be noted that the radial displacements at $\theta = 180°$ for $\mu = 0.4$ and 0.8 are negative. This implies a concave deformed crack-tip profile in contrast to that of $\mu = 0$. The opening profiles of the crack faces will be presented in Fig. 6 and will be discussed later. It should be noted here that there are no HRR-type solutions available for power-law hardening materials based on the original Drucker–Prager yield criterion with $n = 10$ and $\mu = 0.4$ and 0.8.

Figure 5 shows the generalized effective stress contours in the normalized coordinates for various μ's, n's and γ's. These contours can be regarded as approximate plastic zones under small-scale yielding conditions. Figures 5(a) and 5(b) show that the approximate plastic zone shifts toward the front of the tip and stretches in the crack-line direction for large μ as n increases. Figures 5(b) and 5(c) show that the contour shifts backward for large μ as γ decreases. The elongated phase transformation zones in the crack-line direction on the surfaces of three-point bend specimens of zirconia ceramics was observed by Yu and Shetty (1989). We can not directly compare our approximate plastic zone under plane strain conditions with the experimental observation on the surface of specimen under plane stress conditions. The elongated phase transformation zone has been simulated successfully by finite element computations in Ben-Aoun and Pan (1996) based on the original Drucker–Prager yield criterion and by considering the constraint conditions in terms of the T stress. The general trend of our approximate plastic zones for materials with large pressure sensitivity agrees with that of the computational results of shear yielding zones in rubber-

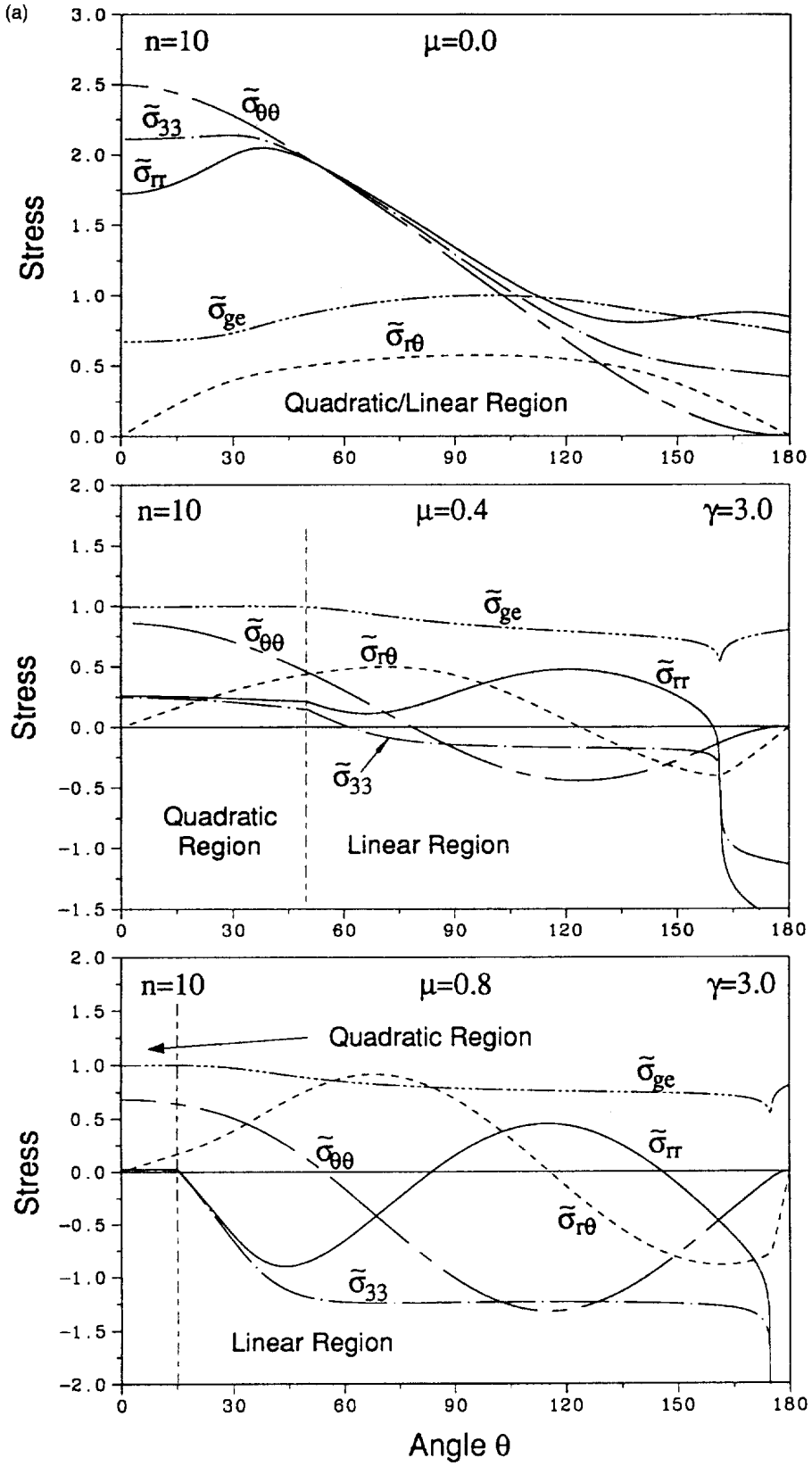

Fig. 4. The angular distributions of the normalized crack-tip stresses, strains, and displacements for $n = 10$, $\gamma = 3$, and $\mu = 0$, 0.4, and 0.8. (*Continued opposite and overleaf.*)

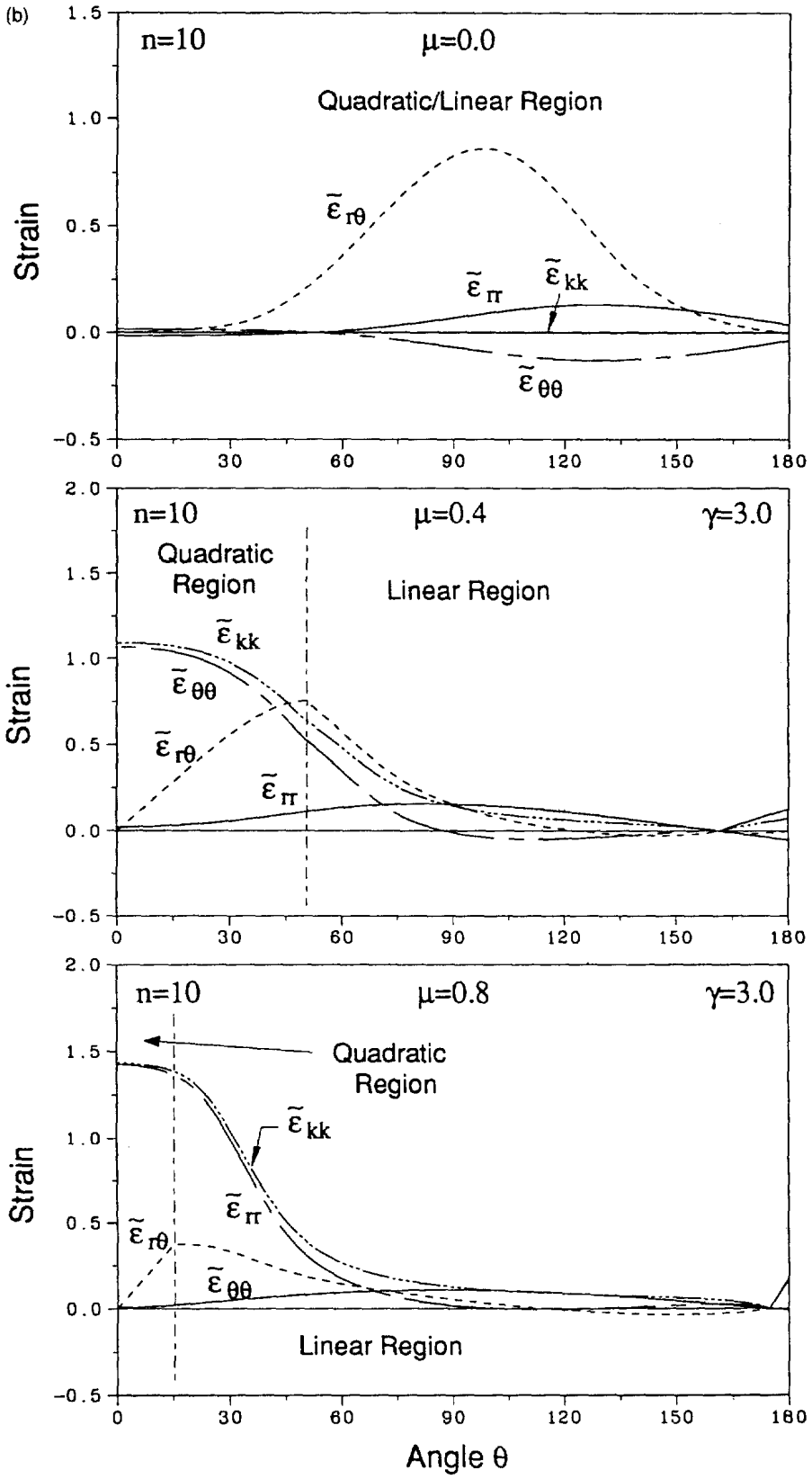

Fig. 4—*Continued.*

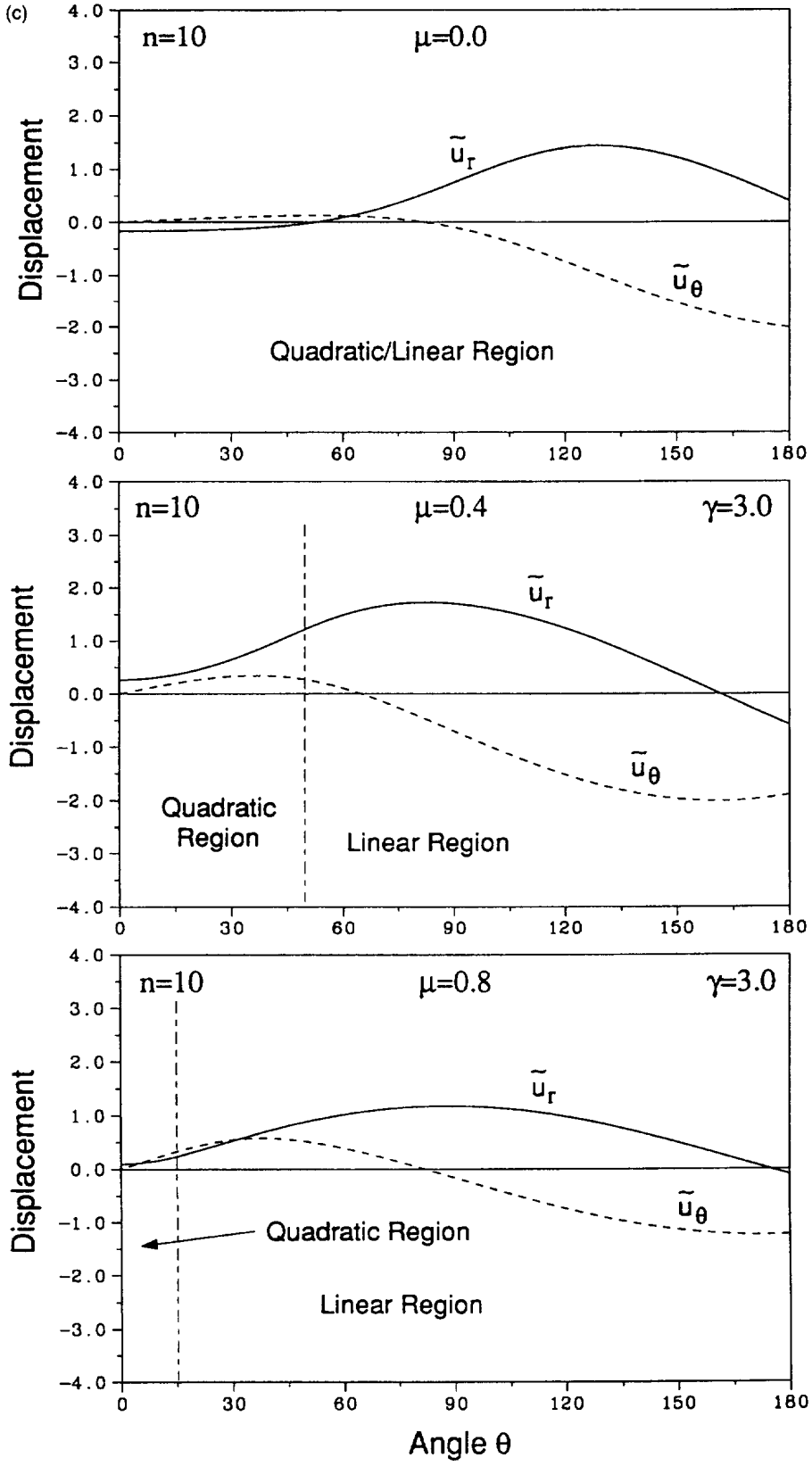

Fig. 4—*Continued.*

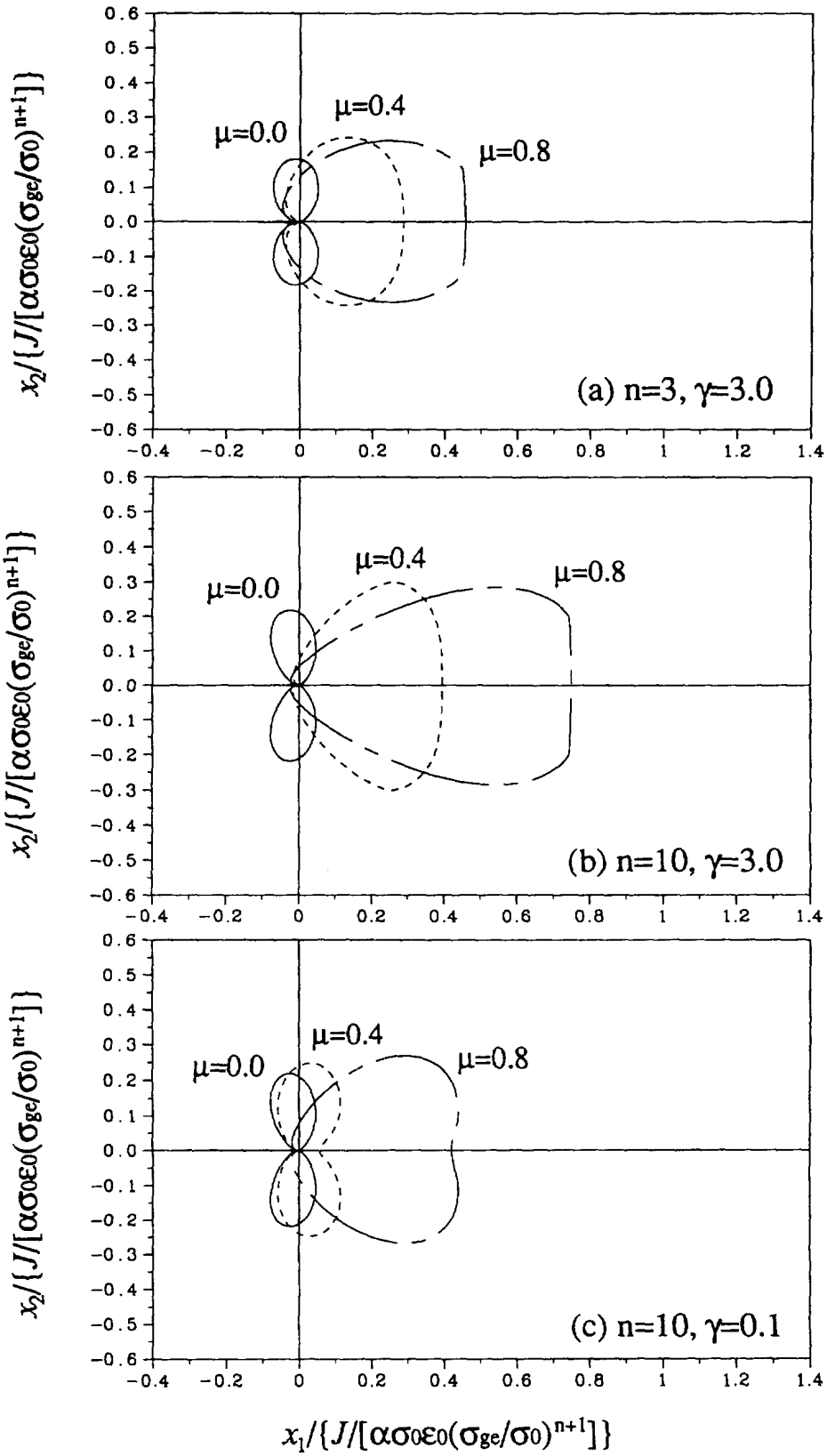

Fig. 5. The generalized effective stress contours in the normalized coordinates for (a) $n = 3$ and $\gamma = 3$, (b) $n = 10$ and $\gamma = 3$, (c) $n = 10$ and $\gamma = 0.1$.

modified epoxies presented in Jeong and Pan (1996). Also, the general trend of our approximate plastic zones for low hardening materials with large pressure sensitivity and small γ's agrees well with the computational results based on the original Drucker–Prager yield criterion for perfectly plastic materials in Kim and Pan (1994) and for strong phase transformation materials in Kim and Pan (1993). The implications of the near-tip fields on fracture of phase transformation ceramics with large μ are discussed in Kim and Pan (1993, 1994).

Figure 6 shows the normalized crack opening profiles for $\gamma = 3$ and $n = 3$, 10, and 50. The length scale used for normalizing the opening shape is the crack opening displacement δ_t as defined earlier. Figure 6 shows that the crack opening profile is convex for $\mu = 0$ and concave for $\mu = 0.4$ and 0.8. The concavity of the crack opening profile decreases as μ changes from 0.4 to 0.8. The concavity of the crack opening profile can be explained by positive $\tilde{u}_1$ and $\tilde{u}_2$ (or negative $\tilde{u}_r$ and $\tilde{u}_\theta$ at $\theta = \pi$). Consider the cases where both $\tilde{u}_1$ and $\tilde{u}_2$ are positive. From eqns (35) and (36), both x_1/δ_t and x_2/δ_t are positive at very small r/δ_t. Therefore, the crack opening profile extends in the first quadrant as r/δ_t increases from 0. When r/δ_t becomes much larger than 1, x_1/δ_t becomes negative. However, x_2/δ_t remains positive. This means the crack opening profile should be in the second quadrant at large r/δ_t. Therefore, the crack opening profile is concave for positive $\tilde{u}_1$ and $\tilde{u}_2$. As shown in Fig. 6, when n increases, the crack opening profile becomes sharper. The concave shape of the crack opening profile suggests that new stress concentration could be generated and, consequently, crack branching may be favorable. The dimensionless constant I in eqn (24) and β in eqn (33) are listed in Table 2 for $\gamma = 3$ with different n's and μ's. In general, as μ increases, I decreases and β increases. As n increases, both I and β decrease.

Crack-tip fields for various values of γ have been obtained to understand the effects of γ on the crack-tip fields. Only a few representative crack-tip fields will be shown here. The crack-tip stress and strain fields for $n = 10$ and $\gamma = 0.1$ are shown in Figs 7(a) and 7(b), respectively, for comparison with those in Fig. 4 for $n = 10$ and $\gamma = 3$. For the $\mu = 0$ case, the stress and strain solutions are the same as those of $\mu = 0$ as shown in Fig. 4 and are not shown here. An examination of the solutions shown in Fig. 7(a) and other solutions for different combinations of n, μ and γ indicates two types of solution structures for the crack-tip fields. The first one is similar to those found by Li and Pan (1990a) and is in general for small γ, small μ, and/or large n. This Prandtl-type crack-tip field has no rapid variation of σ_{rr} near $\theta = 180°$ and σ_{rr} is positive at $\theta = 180°$. The other type is similar to the plane-stress type illustrated in Fig. 4(a) for $\mu = 0.4$ and 0.8. This type has a rapid variation of σ_{rr} near $\theta = 180°$, and σ_{rr} is negative at $\theta = 180°$. For convenience, we refer the former one (the Prandtl type) as type A and the latter one (the plane-stress type) as type B. The conditions in terms of n, μ, and γ for either type A or type B solution can somehow be realized by referring to Table 1. Type A solutions exist under $\gamma \leqslant \gamma_{cr}(n, \mu)$ and can extend to some range of γ above $\gamma_{cr}(n, \mu)$. When the solution is a type A and γ is larger than γ_{cr}, we get a combination of the linear and quadratic regions. The quadratic region appears right ahead of the crack tip. For example, a type A solution for $n = 10$, $\mu = 0.4$ and $\gamma = 0.1$ with a quadratic region ahead of the crack tip is shown in Fig. 7(a). When we decrease γ to zero and keep n and μ constant, the yield criterion approaches to the original Drucker–Prager yield criterion. For the given n and μ, when we do not have any available HRR-type solution based on the original Drucker–Prager yield criterion, the solution is very likely to stay as a type B solution when we decrease γ to a very small value. We have also observed that when the solution becomes a type A as we reduce γ close to 0, the stress state ahead of the crack tip becomes closer to purely hydrostatic.

A comparison of Figs 7(b) and 4(b) shows the tendency of plastic deformation shifting backward when the value of γ decreases. This is especially obvious for the case of $\mu = 0.4$. The plastic deformation concentrates near 90° for $\mu = 0.4$ and $\gamma = 0.1$ shown in Fig. 7(b); whereas the plastic deformation concentrates right in front of the crack tip for $\mu = 0.4$ and $\gamma = 3$ shown in Fig. 4(b). The effects of γ on the strain field is less substantial for large μ as shown in Figs 7(b) and 4(b) for $\mu = 0.8$. For $\mu = 0.8$, the large pressure sensitivity is already strong enough to shift the plastic deformation to the front of the crack tip even without a quadratic part of the yield criterion.

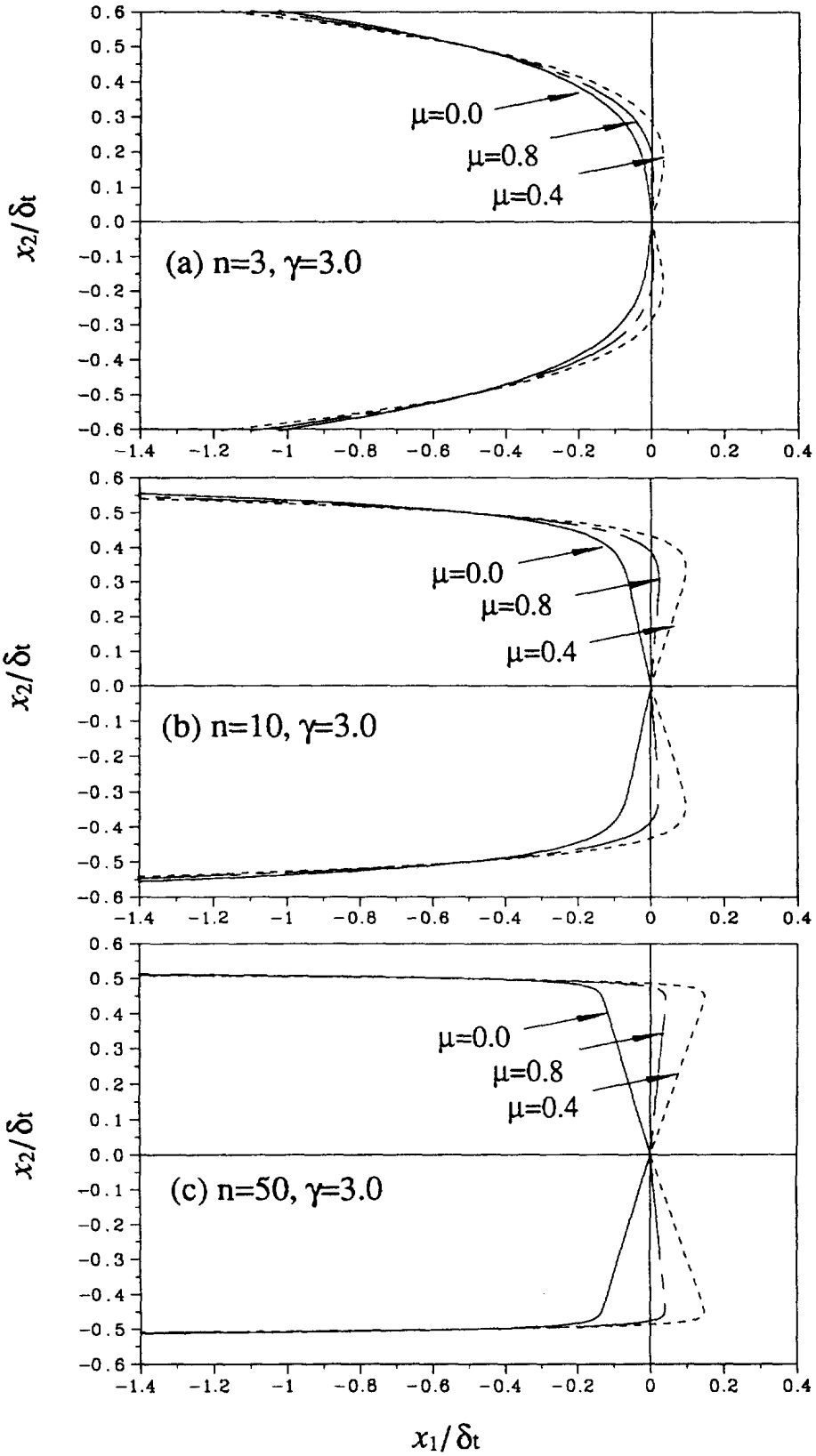

Fig. 6. The crack opening profiles normalized by the crack tip opening displacement for $\gamma = 3$. (a) $n = 3$, (b) $n = 10$, (c) $n = 50$.

Table 2. The numerical values of $\beta(n, \mu)$ and $I(n, \mu)$ for $\gamma = 3$

	$n = 3$		$n = 10$		$n = 50$	
μ	I	β	I	β	I	β
0	5.5073	1.3263	4.5400	0.9314	3.9512	0.8176
0.2	3.9045	2.1353	3.0370	1.4471	2.6758	1.1975
0.4	3.2857	2.6417	2.3469	1.7636	2.0147	1.4539
0.8	2.2956	2.7310	1.3012	1.9341	1.0059	1.6800

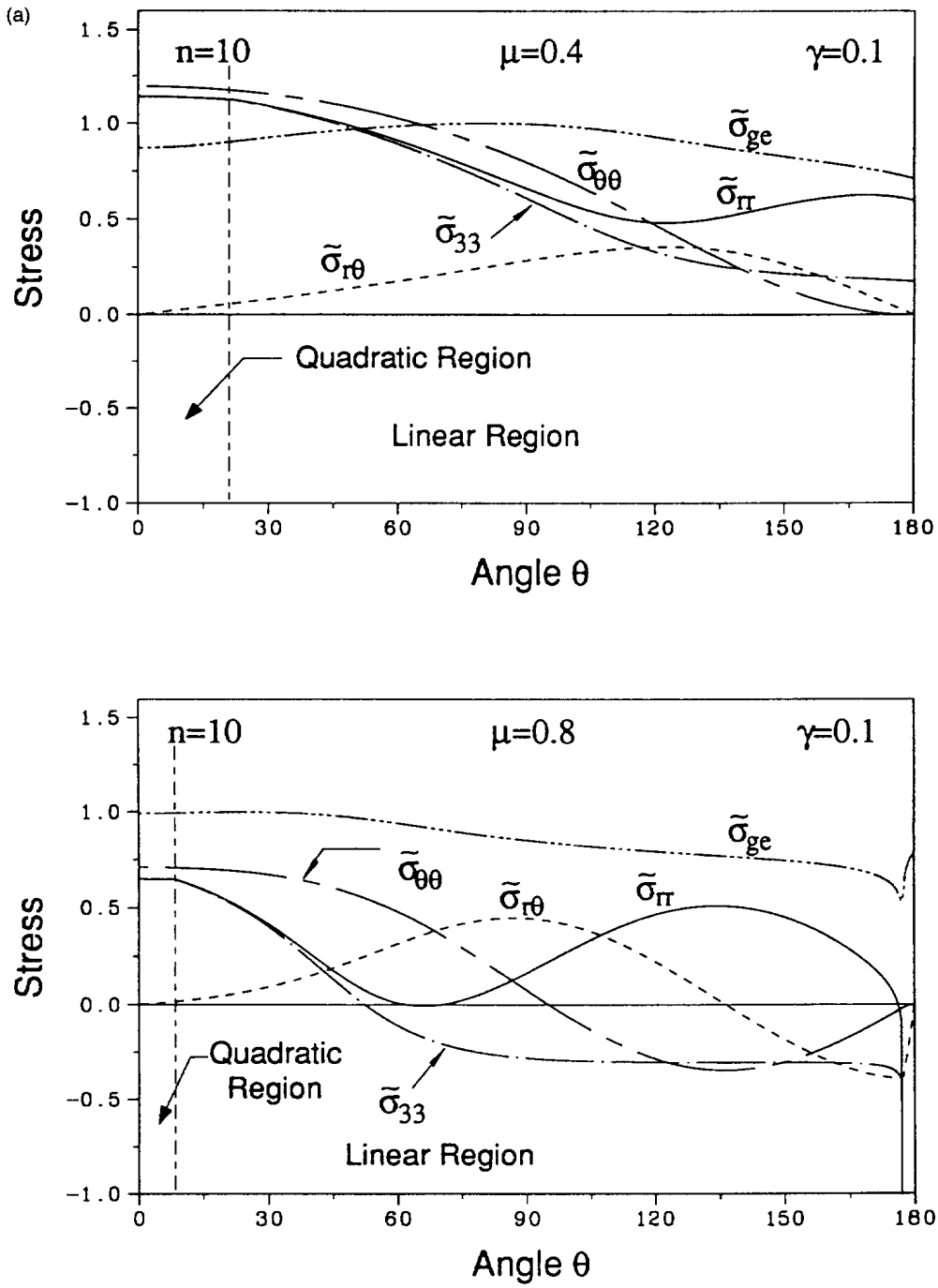

Fig. 7. (a) The normalized crack-tip stresses as functions of θ for $n = 10$, $\gamma = 0.1$, and $\mu = 0.4$ and 0.8; (b) the normalized crack-tip strains as functions of θ for $n = 10$, $\gamma = 0.1$, and $\mu = 0.4$ and 0.8.
(*Continued opposite.*)

(b)

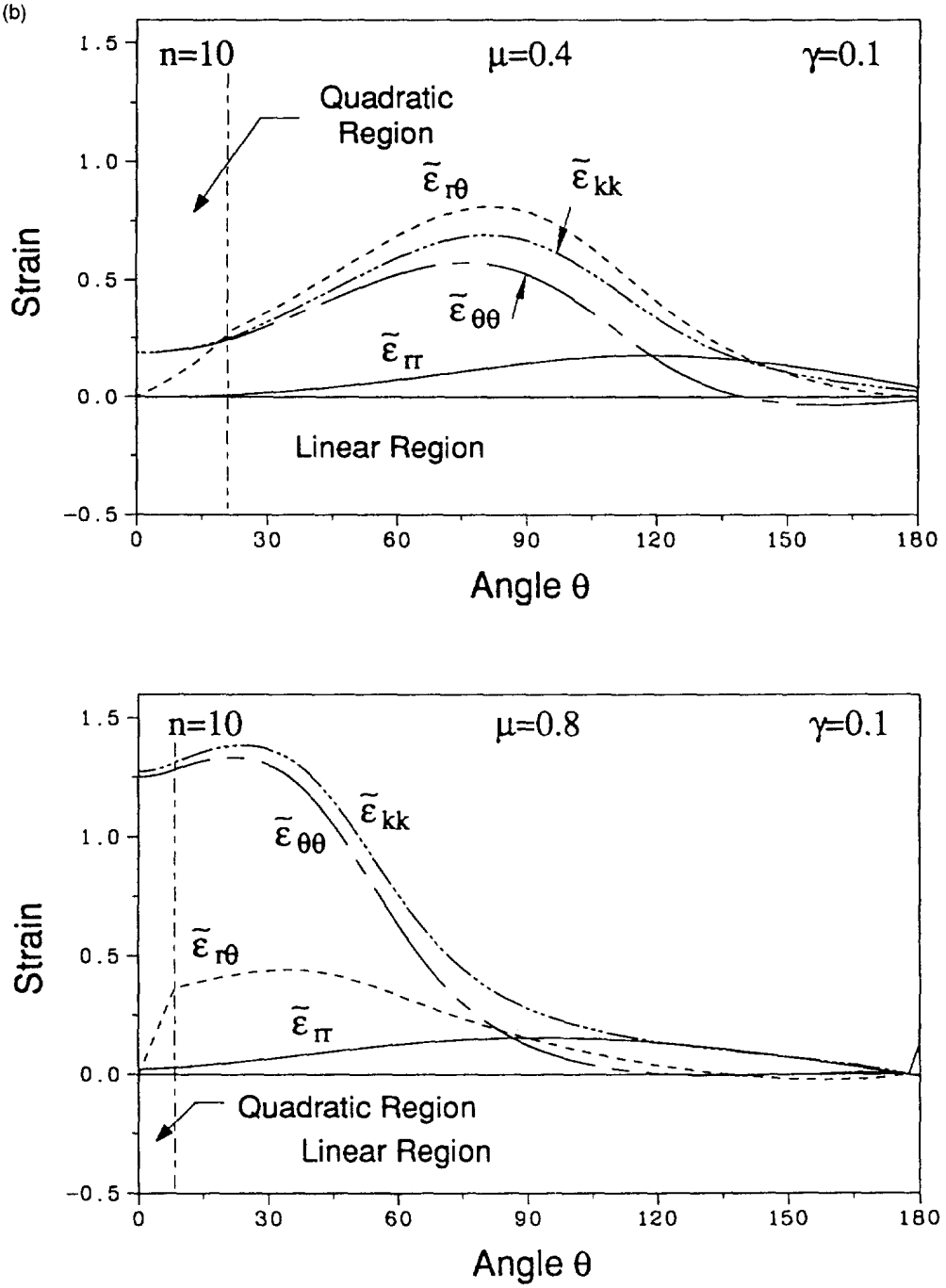

Fig. 7—*Continued.*

In summary, as the ratio γ approaches to 0, the modified Drucker–Prager yield criterion approaches to the original Drucker–Prager yield criterion. Under this condition, the stress state ahead of the tip for power-law hardening materials approaches to purely hydrostatic tension for μ larger than μ_{lim} of Li and Pan (1990a) for a given hardening exponent n. We have tried to obtain the asymptotic solution based on the original Drucker–Prager materials for $\mu > \mu_{lim}$ with the assumption of a state of purely hydrostatic tension at $\theta = 0^\circ$. Since the governing equation of the Airy stress function $\tilde{\phi}$ in eqn (25) for purely hydrostatic tension is singular, we perturbed $\tilde{\phi}$, $\tilde{\phi}'$, $\tilde{\phi}''$ and $\tilde{\phi}'''$ from the state of purely hydrostatic tension at $\theta = 0^\circ$ to a small angle θ by Taylor's expansion to the first order as the boundary

conditions for numerical integration. The numerical integration and shooting for these calculations are quite unstable. However, the available results of the crack-tip fields agree with the finite element solutions of Pan and Chen (1991).

We also note that σ_{rr} near $\theta = 180°$ is negative and its magnitude becomes large as μ becomes close to $\sqrt{3}/2$ for type B solutions. The solution for $\mu = \sqrt{3}/2$ seems not to be accessible for any n and γ except for those solutions by Dong and Pan (1991) for perfectly-plastic materials based on the original Drucker–Prager yield criterion ($\gamma = 0$). This can be explained as follows. The boundary conditions at $\theta = 180°$ require either a plane-strain uniaxial tensile or compressive state. However, the material will not be able to yield under this particular loading condition. In other words, the stress free boundary conditions at $\theta = 180°$ require

$$\sigma_{r\theta} = \sigma_{\theta\theta} = 0.$$

When the material at $\theta = 180°$ follows the linear part of the yield criterion, the generalized effective stress σ_{ge}, according to equation (12), can be represented as

$$\sigma_{ge} = \frac{\sqrt{3}}{2}\left\{\mu + \text{sign}(\sigma_{rr})\left(1 - \frac{\mu^2}{3}\right)^{1/2}\right\}\sigma_{rr} \tag{37}$$

where $\text{sign}(\delta_{rr}) = 1$ when $\sigma_{rr} > 0$ and $\text{sign}(\sigma_{rr}) = -1$ when $\sigma_{rr} < 0$. As μ approaches $\sqrt{3}/2$, the generalized effective stress σ_{ge} becomes zero if we assume that $\sigma_{rr} < 0$ at $\theta = 180°$. In our formulation, when $\sigma_{ge} \leqslant 0$, no plastic flow should occur. This implies that elasticity should play an important role when μ approaches to $\sqrt{3}/2$ or possibly when μ is larger than $\sqrt{3}/2$. Indeed, the finite element computations of Pan and Chen (1991) indicate that for power-law hardening materials, as μ becomes larger than $\sqrt{3}/2$, σ_{ge} becomes negative and only elastic deformation can occur near $\theta = 180°$. Of course, if the stress state is tensile at $\theta = 180°$, the former argument is not true.

5. CRACK-TIP FIELDS FOR PERFECTLY PLASTIC MATERIALS

The development of crack-tip fields for perfectly-plastic materials based on the modified Drucker–Prager yield criterion follows the work of Rice (1982). The asymptotic equilibrium equations given by Rice (1982) are

$$\frac{\partial \sigma_{r\theta}}{\partial \theta} + \sigma_{rr} - \sigma_{\theta\theta} = 0 \tag{38}$$

$$\frac{\partial \sigma_{\theta\theta}}{\partial \theta} + 2\sigma_{r\theta} = 0. \tag{39}$$

The yield function for perfectly plastic materials can be expressed as

$$\psi(\sigma_{ij}) = \sigma_0 \tag{40}$$

where σ_0 is a constant. Rice (1982) defined a singular plastic sector where in-plane strain components develop singularity at the tip as $r \to 0$. The in-plane strain singularity leads to

$$P_{33} = 0 \tag{41}$$

where $P_{33} = \partial\psi/\partial\sigma_{33}$. The governing equation derived from the yield criterion and equilibrium equations for singular plastic sectors is

$$\frac{\mathrm{d}(\sigma_{11}+\sigma_{22})}{\mathrm{d}\theta} P_{rr} = 0 \tag{42}$$

where $P_{rr} = \partial\psi/\partial\sigma_{rr}$. From eqn (42), the solution can be classified into two types:

(1) Constant stress sectors (these sectors are governed by $\mathrm{d}(\sigma_{11}+\sigma_{22})/\mathrm{d}\theta = 0$ which leads to σ_{11} = constant, σ_{12} = constant, σ_{22} = constant, and σ_{33} = constant. Also, σ_{11}, σ_{12}, σ_{22}, and σ_{33} satisfy eqns (40) and (41)).
(2) Centered fan sectors (these sectors are governed by $P_{rr} = 0$. Also, eqns (38), (39) and (41) have to be satisfied).

Our yield criterion consists of a linear part and a quadratic part. Therefore we can have four types of singular plastic sectors: quadratic constant stress sector (QCS), quadratic centered fan sector (QCF), linear constant stress sector (LCS), and linear centered fan sector (LCF).

For perfectly plastic materials the assemblies of crack-tip fields are generally non-unique. Our assembled perfectly plastic solutions correspond to the perfectly plastic limits of power-law hardening solutions. These solutions represent rigid perfectly plastic solutions. It should be noted that elastic sectors may appear near the tip for elastic perfectly plastic materials, see Kim and Pan (1994). From the low-hardening solutions, we can identify the possible appearance of constant stress sectors, and decide the relative placement of these singular plastic sectors. For $\mu = 0$, starting from $\theta = 0^\circ$ to 180° there is a constant stress sector, a centered fan sector, and then another constant stress sector bordering the crack surface. This is a type A crack-tip field as discussed earlier for power-law hardening materials. The crack-tip field for $\mu = 0$ is exactly the same as the Prandtl field. As μ increases, another type of crack-tip structure emerges. The stress field becomes, starting from $\theta = 0^\circ$ to 180°, a possible QCS, a QCF, a LCF, a LCS, and another LCS. When a QCS is considered to exist in front of the crack tip, the assembled solution becomes non-unique. After a close examination of our low-hardening solutions, we find it is obvious that σ_{rr} and σ_{33} are nearly identical at $\theta = 0^\circ$. Note that $\sigma_{rr} = \sigma_{33}$ is a feature of a centered fan sector. We hence decide that in front of the crack tip a centered fan should appear. This is a type B field as discussed earlier for power-law hardening materials. We referred to this type of crack-tip field as a plane-stress type because the structure is similar to the crack-tip field for Mises materials under plane stress conditions (Hutchinson, 1968b). These two types of crack-tip structures are schematically shown in Figs 8(a) and 8(b).

The assembly of different sectors requires that $\sigma_{r\theta}$ and $\sigma_{\theta\theta}$ along the borders of two different sectors be continuous. A significant feature of a centered fan sector, either a linear or a quadratic centered fan sector, is that σ_{rr} has to be continuous along the border with other plastic sectors. The reason for the continuity of σ_{rr} is that $P_{rr} = 0$ enforces the stress component σ_{rr} to be determined within the centered fan sector as a double root of a quadratic polynomial equation (Kim and Pan, 1994). The consequence is that we can only have radial stress discontinuity along the border between two constant stress sectors.

The solutions for singular plastic sectors based on the quadratic part of the modified Drucker–Prager yield criterion are detailed in Appendix A. The solutions for singular plastic sectors based on the linear part of the modified Drucker–Prager yield criterion are the same as those based on the original Drucker–Prager yield criterion. The solutions can be found in Kim and Pan (1994). Based on the closed-form solutions, the crack-tip fields are assembled according to Figs 8(a) and 8(b), depending on the corresponding low-hardening solutions. The normalized crack-tip stress $\tilde{\sigma}_{ij}$ $(=\sigma_{ij}/\sigma_0)$ as functions of θ for perfectly-plastic materials with $\mu = 0.01$, 0.4 and 0.8 are presented in Figs 9(a) and 9(b) for $\gamma = 3$ and 0.1, respectively. For $\mu = 0$, the yield criterion becomes the Mises yield criterion. Therefore the solution is the Prandtl solution, independent of the value of γ. Here we plot the solutions for a small μ $(=0.01)$ for completeness. Due to the large value of $\gamma = 3$, the

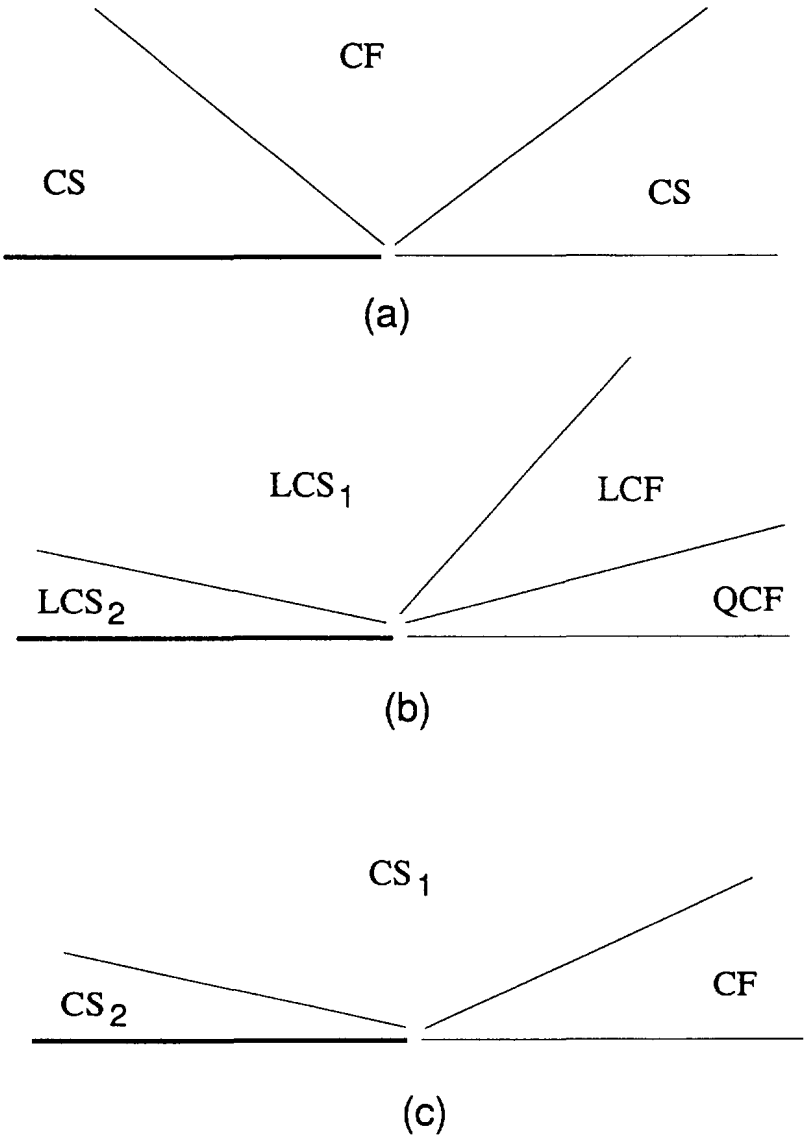

Fig. 8. The schematic plots of different assemblies of singular plastic sectors for crack-tip fields for perfectly plastic materials.

solution for $\mu = 0.01$ shown in Fig. 9(a) is entirely based on the quadratic part of the yield criterion. However, as γ decreases to 0.1, the solution for $\mu = 0.01$ shown in Fig. 9(b) is determined completely by the linear part of the yield criterion. The perfectly-plastic stress solutions agree well with our low-hardening solutions. Thus our low-hardening solution and perfectly plastic solution validate each other. Note that the solution shown in Fig. 9(b) for $\mu = 0.4$ and $\gamma = 0.1$ is a type A field. The solution is the same as that based on the original Drucker–Prager yield criterion because γ $(=0.1)$ is smaller than γ_{cr} $(=0.1537)$ as listed in Table 1. From Figs 9(a) and 9(b), we also find that the stress states ahead of the crack tip for a given μ are apparently different for different values of γ. This conclusion is the same as that for power-law hardening materials. This indicates the necessity to accurately determine the yield criterion at small values of σ_e/σ_m, possibly by analytical or computational methods in view of the difficulty of experimental methods.

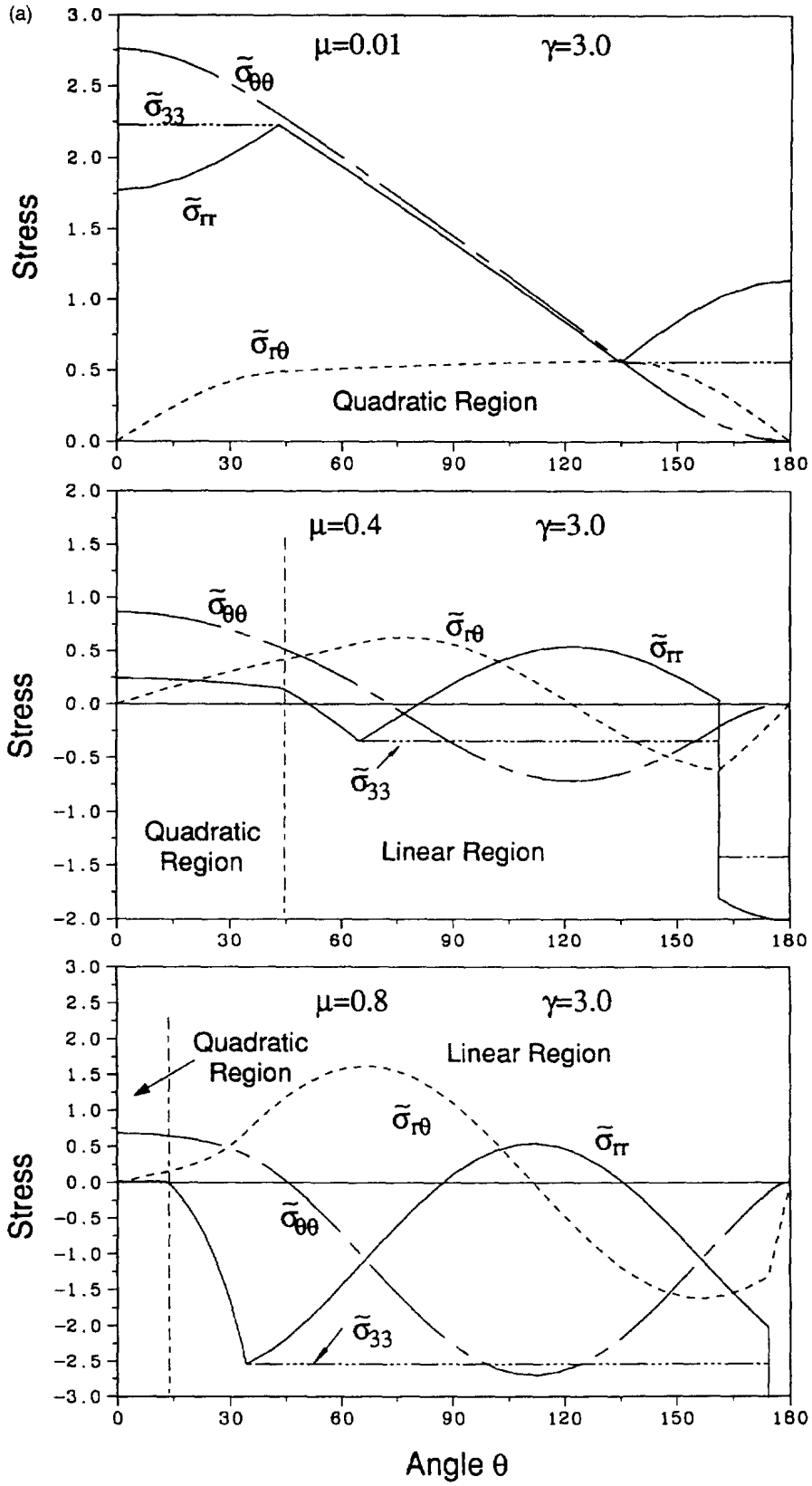

Fig. 9. The normalized crack-tip stresses as functions of θ for perfectly plastic materials with $\mu = 0.01$, 0.4, and 0.8 (a) $\gamma = 3$, (b) $\gamma = 0.1$. (*Continued overleaf.*)

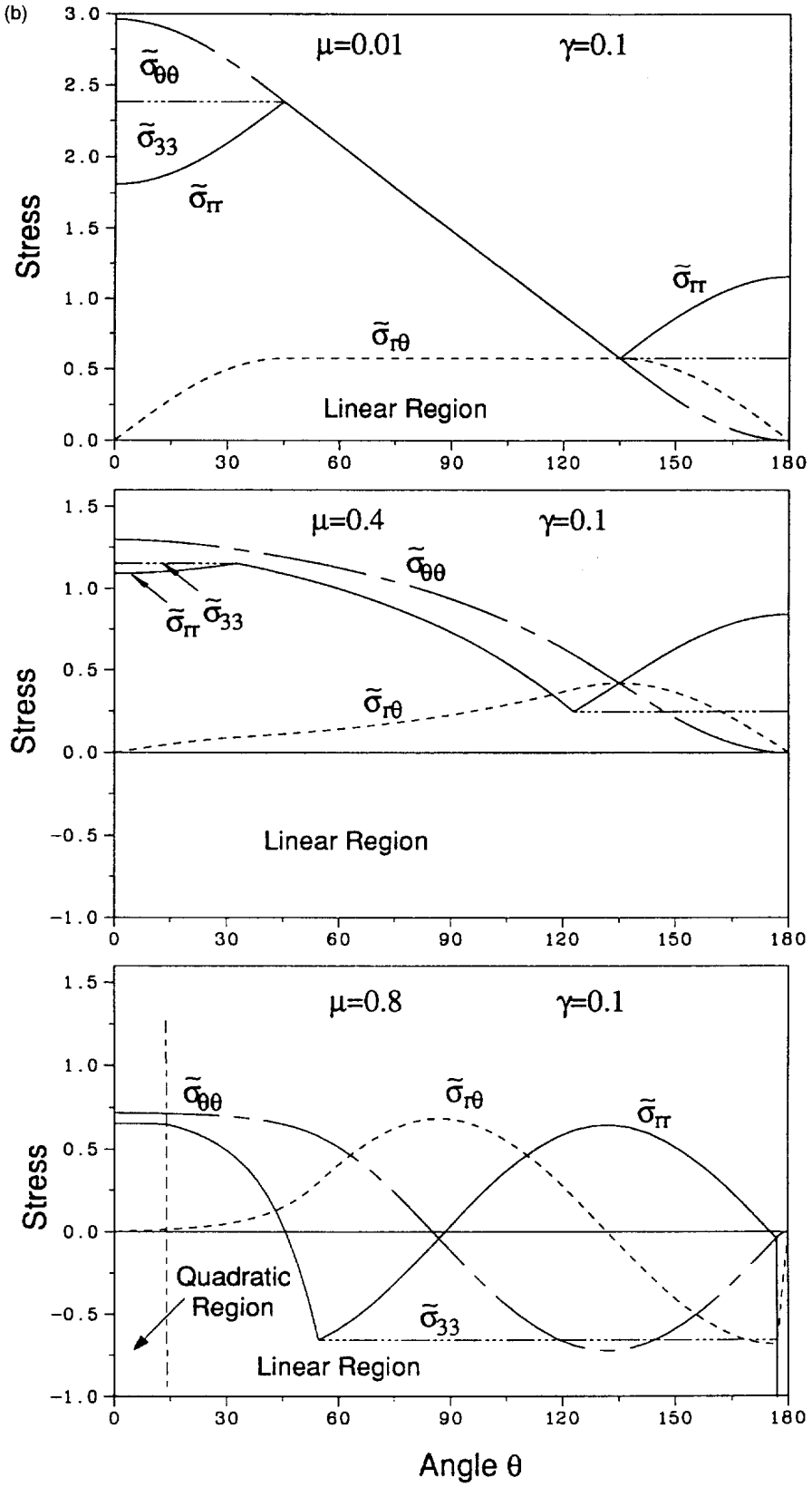

Fig. 9—*Continued.*

Provided that the structure of the crack-tip fields remains as that in Fig. 8(b) as γ decreases to 0, the constraint $P_{rr} = 0$ for the QCF sector leads to the stress state at $\theta = 0^\circ$ as

$$\sigma_{11} = \left(\frac{9A-2B}{9A+4B}\right)\sigma_{22}. \tag{43}$$

Substituting eqn (43) into the yield criterion (A9) and considering the symmetry condition $\sigma_{12} = 0$ at $\theta = 0^\circ$, we arrive at

$$\sigma_{11}(\theta = 0^\circ) = \frac{\kappa\sigma_0}{\sqrt{\beta_1(\kappa^2+1)+\beta_2\kappa}} \tag{44}$$

$$\sigma_{22}(\theta = 0^\circ) = \frac{\sigma_0}{\sqrt{\beta_1(\kappa^2+1)+\beta_2\kappa}} \tag{45}$$

where

$$\beta_1 = \frac{3}{4}A\left(\frac{9A+4B}{9A+B}\right), \quad \beta_2 = -\frac{3}{2}A\left(\frac{9A-2B}{9A+B}\right) \quad \text{and} \quad \kappa = \frac{9A-2B}{9A+4B}.$$

Examining eqn (43) when γ approaches 0, we find that

$$\sigma_{11}/\sigma_{22} \to 1 \quad \text{at} \quad \theta = 0^\circ \quad \text{as} \quad \gamma \to 0. \tag{46}$$

A purely hydrostatic tension should be expected at $\theta = 0^\circ$ under the assumption that the solution structure stays as that shown in Fig. 8(b). This conclusion is essentially the same as that from the finite element computations of Pan and Chen (1991) for hardening materials based on the original Drucker–Prager yield criterion.

Another parabolic type of yield criterion similar to our modified Drucker–Prager yield criterion has been used to characterize the yielding behavior of plastics (Raghava *et al.*, 1973; Caddell *et al.*, 1974). This yield criterion has the form of

$$\psi(\sigma_{ij}) = \sigma_e^2 + c\sigma_m = \sigma_0'^2 \tag{47}$$

where c and σ_0' are two material constants and can be related to the magnitudes of the uniaxial tensile and compressive yield stresses, σ_t and σ_c, as

$$c = 3(\sigma_c - \sigma_t), \quad \sigma_0'^2 = \sigma_c\sigma_t. \tag{48}$$

Note that the constant σ_0' is different from the material constant in the modified Drucker–Prager yield criterion in eqns (3) and (4) with $\sigma_{ge} = \sigma_0$. Since the parabolic yield criterion in eqn (47) does not have the same order of power for σ_e and σ_m, the HRR-type solutions for power-law hardening materials cannot be formulated. One way of developing perfectly plastic solutions based on the parabolic yield criterion is to perform a finite element analysis and examine the structures of the crack-tip fields from the computational results. However, we take the advantage of the fact that the geometric shape of the modified Drucker–Prager yield criterion with $\gamma = 3$ in the σ_m–σ_e plane is similar to that based on the parabolic yield criterion. We therefore expect that the structures of the crack-tip fields based on the parabolic yield criterion are similar to those based on the modified Drucker–Prager yield criterion with $\gamma = 3$. From the results for materials based on the modified Drucker–Prager yield criterion, we expect two types of crack-tip fields based on the parabolic yield criterion.

Type A is similar to the Prandtl yield as shown in Fig. 8(a). Type B is similar to the plane-stress type of crack-tip field as shown in Fig. 8(c). Closed-form solutions for singular plastic sectors based on the parabolic yield criterion are detailed in Appendix A.

The assembly of the crack-tip fields follows the same procedure for materials based on the modified Drucker–Prager yield criterion. Figure 10 shows the normalized stresses $\tilde{\sigma}_{ij}$ $(=\sigma_{ij}/\sigma_0')$ as functions of θ based on the parabolic yield criterion with the same uniaxial tensile and compressive yield stresses as those for materials based on the modified Drucker–Prager yield criterion with $\mu = 0.01$, 0.4 and 0.8. For materials corresponding to $\mu = 0.01$, we have a type A structure. For materials corresponding to $\mu = 0.4$ and 0.8, we have type B structures. As shown in Figs 10 and 9(a), the stress solutions based on the modified Drucker–Prager yield criterion with $\gamma = 3$ and the parabolic yield criterion are quite different, especially the stresses ahead of the crack tip at $\theta = 0°$. The stresses ahead of the tip at $\theta = 0°$ are important parameters for crack initiation and growth. Consequently, the exact geometry of the yield surface, especially at large ratio of σ_m/σ_e, is critical to the analysis of crack initiation and growth.

For materials based on the modified Drucker–Prager yield criterion, when the pressure sensitivity becomes large and the quadratic portion of the yield contour increases, Type B (plane-stress type) crack-tip fields emerge. For Type B crack-tip fields, radial stress discontinuity occurs along the border between the two constant stress sectors and the sector bordering the crack face is under plane strain compression in the crack-line direction. For perfectly plastic materials, the yield criterion at $\theta = 180°$ follows eqn (37) with σ_{ge} being a constant. At $\theta = 180°$, σ_{rr} is negative for Type B crack-tip fields. As μ approaches $\sqrt{3}/2$, the factor in the curly braces in eqn (37) approaches to zero. Then σ_{rr} has to approach to infinity to satisfy the yield criterion. This trend is shown in Figures 9(a) and 9(b). This is one consequence of the assumption that yielding occurs at all angles around the tip. However, the computational results of the mixed-mode crack-tip fields for Mises materials (Dong and Pan, 1990a, 1990b) indicate that when elasticity is considered, the radial stress discontinuity of fully-yielded crack-tip fields disappears and a finite-stress elastic sector appears in the neighborhood. Therefore when we include the elastic behaviour in our perfectly plastic analysis, the radial stress discontinuity and the large negative radial stress near the crack face should disappear. For materials based on the parabolic yield criterion, when the pressure sensitivity increases, Type B crack-tip fields also emerge. However, as the pressure sensitivity increases, the radial stress at $\theta = 180°$ does not have the type of behavior near $\mu = \sqrt{3}/2$ as specified in eqn (37) for materials based on the modified Drucker–Prager yield criterion.

6. CONCLUSION

We have proposed a modified Drucker–Prager yield criterion which consists of a linear function and a quadratic function of the tensile effective stress and the mean stress in order to understand the effects of the vertex on the yield surface based on the original Drucker–Prager yield criterion. We find that the HRR-type asymptotic crack-tip fields can be found based on the modified Drucker–Prager yield criterion whereas the solution procedure breaks down on the original Drucker–Prager yield criterion. We also present the crack-tip fields for perfectly plastic materials based on the modified Drucker–Prager yield criterion and a parabolic type of yield criterion. The asymptotic crack-tip solutions for both power-law hardening and perfectly-plastic materials suggest that the crack-tip stress distribution depends on the detailed geometric shape of the yield surface near the state of purely hydrostatic tension. More research is needed to shed light on the yield behavior at large mean stresses for pressure-sensitive materials in order to understand fracture of these materials.

Acknowledgements—The financial support of this work was provided by the NSF under grant number DMR-8708405 and DMR-9119598. Helpful discussions with Professor I. W. Chen of the University of Michigan are appreciated.

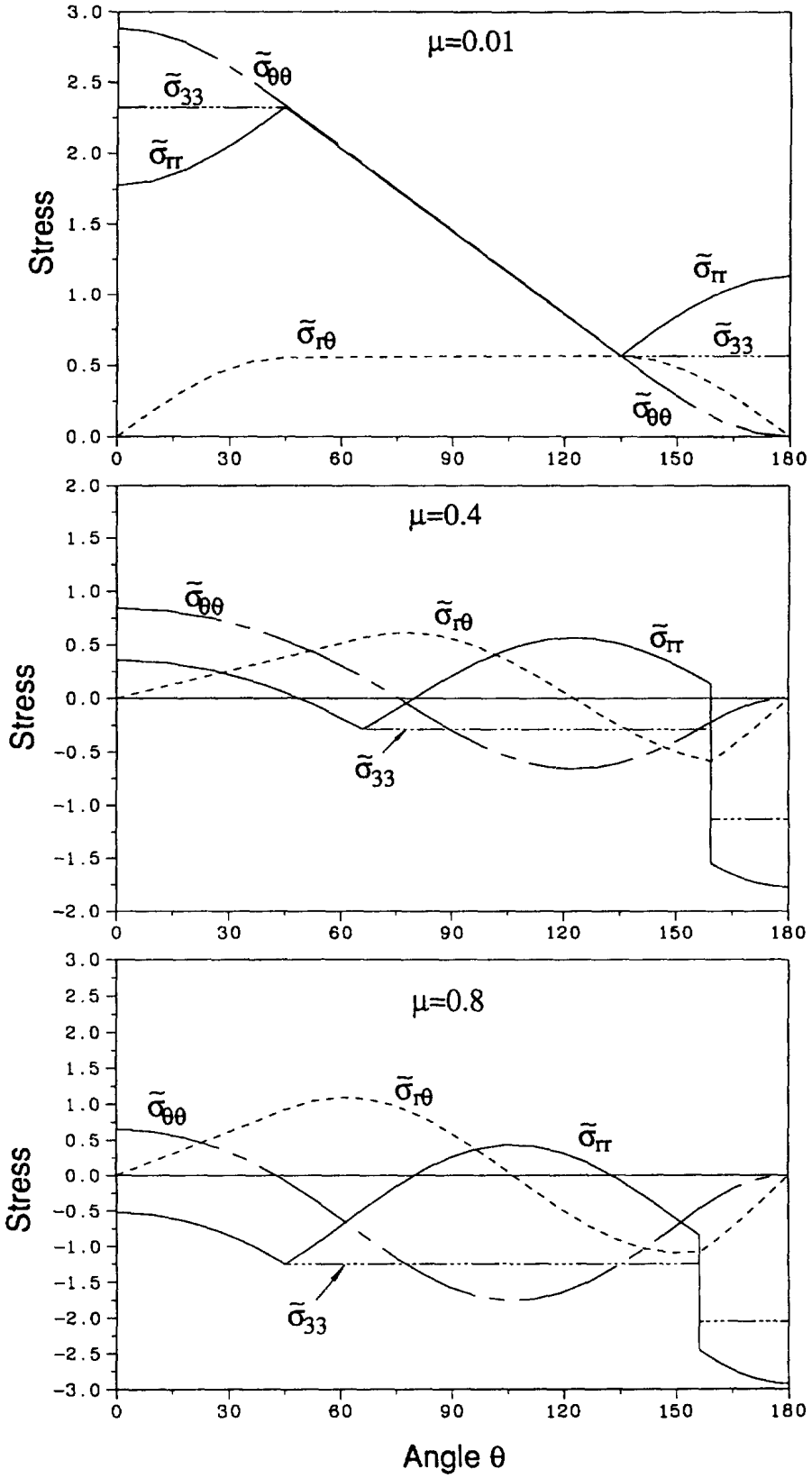

Fig. 10. The normalized crack-tip stresses as functions of θ for perfectly plastic materials based on the parabolic yield criterion for $\mu = 0.01$, 0.4, and 0.8.

REFERENCES

Aoki, S., Kishimoto, K., Takeya, A. and Sakata, M. (1984). Effects of microvoids on crack blunting and initiation in ductile materials. *International Journal of Fracture* **24,** 267–278.

Aravas, N. and McMeeking, R. M. (1985). Microvoid growth and failure in the ligament between a hole and a blunt crack tip. *International Journal of Fracture* **29,** 21–38.

Ben-Aoun, Z. and Pan, J. (1996). Influences of non-singular stresses on plane-stress near-tip fields for pressure-sensitive materials and applications to transformation toughened ceramics. *International Journal of Fracture* **77,** 223–241.

Caddell, R. M., Raghava, R. S. and Atkins, A. G. (1974). Pressure dependent yield criteria for polymers. *Materials Science Engineering* **13,** 113–120.

Carapellucci, L. M. and Yee, A. F. (1986). The biaxial deformation and yield behavior of Bisphenol-A polycarbonate: effect of anisotropy. *Polymer Engineering Science* **26,** 920–930.

Chen, I.-W. and Reyes Morel, P. E. (1986). Implications of transformation plasticity in ZrO_2-containing ceramics: I, shear and dilatation effects. *Journal of American Ceramic Society* **69,** 181–189.

Chen, I.-W. (1991). Model of transformation toughening in brittle materials. *Journal of American Ceramic Society* **74,** 2564–2572.

Dong, P. and Pan, J. (1990a). Plane-strain mixed-mode near-tip fields in elastic perfectly plastic solids under small-scale yielding conditions. *International Journal of Fracture* **45,** 243–262.

Dong, P. and Pan, J. (1990b). Plane-stress mixed-mode near-tip fields in elastic perfectly plastic solids. *Engineering Fracture Mechanics* **37,** 43–57.

Dong, P. and Pan, J. (1991). Elastic–plastic analysis of cracks in pressure-sensitive materials. *International Journal of Solids and Structures* **28,** 1113–1127.

Drucker, D. C. (1973). Plasticity theory, strength-differential (SD) phenomenon, and volume expansion in metals and plastics. *Metallurgy Transactions* **4,** 667–673.

Drucker, D. C. and Prager, W. (1952). Soil mechanics and plastic analysis on limit design. *Quarterly Applied Mathematics* **10,** 157–165.

Gurson, A. L. (1975). Plastic flow and fracture behavior of ductile materials incorporating void nucleation, growth, and interaction. Ph.D. thesis, Brown University, Providence, Rhode Island.

Gurson, A. L. (1977). Continuum theory of ductile rupture by void nucleation and growth: Part I—yield criteria and flow rules for porous ductile media. *Journal of Engineering Materials Technology* **99,** 2–15.

Hutchinson, J. W. (1968a). Singular behavior at the end of a tensile crack in a hardening material. *Journal of the Mechanics and Physics of Solids* **16,** 13–31.

Hutchinson, J. W. (1968b). Plastic stress and strain fields at a crack tip. *Journal of the Mechanics and Physics of Solids* **16,** 337–347.

Jeong, H.-Y. and Pan, J. (1995). A macroscopic constitutive law for porous solids with pressure-sensitive matrices and its implications to plastic flow localization. *International Journal of Solids and Structures* **32,** 3669–3691.

Jeong, H.-Y. and Pan, J. (1996). Crack-tip fields for porous solids with pressure-sensitive matrices and for rubber-modified epoxies. *Polymer Engineering Science* **36,** 2306–2319.

Kim, M. and Pan, J. (1993). Effects of non-singular stresses on crack-tip fields for transformation toughened materials: part I—plane strain case. Presented at the *95th Annual Meeting of the American Ceramic Society*, Cincinnati, Ohio, 18–22 April.

Kim, M. and Pan, J. (1994). Effects of non-singular stresses on crack-tip fields for pressure-sensitive materials, part I: plane strain case. *International Journal of Fracture* **68,** 1–34.

Kinloch, A. J. and Young, R. J. (1983). *Fracture Behaviour of Polymers*, Elsevier Applied Science, London.

Li, F. Z. and Pan, J. (1990a). Plane-strain crack-tip fields for pressure-sensitive dilatant materials. *Journal of Applied Mechanics* **57,** 40–49.

Li, F. Z. and Pan, J. (1990b). Plane-Stress crack-tip fields for pressure-sensitive dilatant materials. *Engineering Fracture Mechanics* **35,** 1105–1116.

McMeeking, R. M. (1977). Finite deformation analysis of crack-tip opening in elastic–plastic materials and implications for fracture. *Journal of Mechanics and Physics of Solids* **25,** 357–381.

Needleman, A. and Tvergaard, V. (1987). An analysis of ductile rupture modes at a crack tip. *Journal of Mechanics and Physics of Solids* **35,** 151–183.

Pan, J. and Chen, I.-W. (1991). Crack-tip fields for transformation toughening materials. Presented at the *93rd Annual Meeting of the American Ceramic Society*, Cincinnati, Ohio, 28 April–2 May.

Pearson, R. A. and Yee, A. F. (1991). Influence of particle size and particle size distribution on toughening mechanisms in rubber-modified epoxies. *Journal of Materials Science* **26,** 3828–3844.

Rabinowtz, S., Ward, I. M. and Parry, J. S. C. (1970). The effect of hydrostatic pressure on the shear yield behaviour of polymers. *Journal of Materials Science* **5,** 29–39.

Raghava, R., Caddell, R. M. and Yeh, G. S. Y. (1973). The macroscopic yield behaviour of polymers. *Journal of Materials Science* **8,** 225–232.

Reyes-Morel, P. E. and Chen, I.-W. (1988). Transformation plasticity of CeO_2-stabilized tetragonal zirconia polycrystals: I, stress assistance and autocatalysis. *Journal of American Ceramic Society* **71,** 343–353.

Rice, J. R. (1968). A path independent integral and the approximate analysis of strain concentration by notches and cracks. *Journal of Applied Mechanics* **35,** 379–386.

Rice, J. R. and Rosengren, G. F. (1968). Plane strain deformation near a crack tip in a power-law hardening material. *Journal of Mechanics and Physics of Solids* **16,** 1–12.

Rice, J. R. (1982). Elastic–plastic crack growth. In *Mechanics of Solids: The R. Hill 60th Anniversary Volume* (eds H. G. Hopkins and M. J. Sewell), Pergamon Press, Oxford pp. 539–562.

Sauer, J. A., Pae, K. D. and Bhateja, S. K. (1973). Influence of pressure on yield and fracture in polymers. *Journal of Macromolecular Science–Physics* **B8,** 631–654.

Shih, C. F. (1973). Elastic–plastic analysis of combined mode crack problems. Ph.D. thesis, Harvard University, Cambridge, Massachusetts.

Shih, C. F. (1981). Relationships between the J-integral and the crack opening displacement for stationary and extending cracks. *Journal of the Mechanics and Physics of Solids* **29,** 305–326.

Spitzig, W. A., Sober, R. J. and Richmond, O. (1975). Pressure dependence of yielding and associated volume expansion in tempered matensite. *Acta Metallurgica* **23,** 885–893.
Spitzig, W. A., Sober, R. J. and Richmond, O. (1976). The effect of hydrostatic pressure on the deformation behavior of maraging and HY-80 steels and its implications for plasticity theory. *Metallurgy Transactions* **7A,** 1703–1710.
Spitzig, W. A. and Richmond, O. (1979). Effect of hydrostatic pressure on the deformation behavior of polyethylene and polycarbonate in tension and in compression. *Polymer Engineering Science* **19,** 1129–1139.
Sternstein, S. S. and Ongchin, L. (1969). Yield criteria for plastic deformation of glassy high polymers in general stress fields. *American Chemistry Society Polymers* **10,** 1117–1124.
Tvergaard, V. (1981). Influence of voids on shear band instabilities under plane strain conditions. *International Journal of Fracture* **17,** 389–407.
Tvergaard, V. (1982). On localization in ductile materials containing spherical voids. *International Journal of Fracture* **18,** 237–252.
Whitney, W. and Andrews, R. D. (1967). Yielding of glassy polymers: volume effects. *Journal of Polymer Science: Polymer Symposia* **16C,** 2981–2990.
Yu, C.-S. and Shetty, D. K. (1989). Transformation zone shape, size, and crack-growth-resistance (*R*-curve) behavior of ceria-partially-stabilized zirconia polycrystals. *Journal of the American Ceramic Society* **72,** 921–928.

APPENDIX A: SINGULAR PLASTIC SECTOR SOLUTIONS

In this appendix, we present the solutions of singular plastic sectors for perfectly plastic materials based on the quadratic and parabolic types of yield criteria.

A.1. Quadratic yield criterion

First we examine the solutions based on the quadratic part of the modified Drucker–Prager yield criterion. The yield criterion is defined as

$$\psi(\sigma_{ij}) = (A\sigma_e^2 + B\sigma_m^2)^{1/2} = \sigma_0 \tag{A1}$$

where σ_0 is a material constant, and A and B are defined in eqn (5). The components of the outward normal to the yield surface are

$$P_{ij} = \frac{\partial \psi}{\partial \sigma_{ij}} = \frac{1}{2\sigma_0}(3As_{ij} + \tfrac{2}{3}B\sigma_m \delta_{ij}). \tag{A2}$$

Further, the condition $P_{33} = 0$ leads to

$$\sigma_{33} = \frac{9A-2B}{18A+2B}(\sigma_{11}+\sigma_{22}), \tag{A3}$$

which is exactly the same as eqn (18) for hardening materials.

(1) *Quadratic centered fan sector.* The condition $P_{rr} = 0$ for centered fan sector leads to

$$\sigma_{rr} = \frac{9A-2B}{18A+2B}(\sigma_{11}+\sigma_{22}) = \frac{9A-2B}{18A+2B}(\sigma_{rr}+\sigma_{\theta\theta}). \tag{A4}$$

Combining eqns (A4) and (A3) and solving for σ_{rr} from (A4), we get

$$\sigma_{rr} = \sigma_{33} = \frac{9A-2B}{9A+4B}\sigma_{\theta\theta}. \tag{A5}$$

Substituting the above relation into the equilibrium eqns in (38) and (39), we derive the solutions for centered fan sectors as

$$\sigma_{\theta\theta} = \sigma^0_{\theta\theta}\cos(k(\theta-\theta_0)) - \sqrt{\frac{9A+4B}{3B}}\sigma^0_{r\theta}\sin(k(\theta-\theta_0)) \tag{A6}$$

$$\sigma_{r\theta} = \sqrt{\frac{3B}{9A+4B}}\sigma^0_{\theta\theta}\sin(k(\theta-\theta_0)) + \sigma^0_{r\theta}\cos(k(\theta-\theta_0)) \tag{A7}$$

$$\sigma_{33} = \sigma_{rr} = \frac{9A-2B}{9A+4B}\sigma_{\theta\theta} \tag{A8}$$

where $k = \sqrt{12B/(9A+4B)}$, θ_0 is a reference angle, and $\sigma^0_{r\theta}$ and $\sigma^0_{\theta\theta}$ are the stress components at $\theta = \theta_0$.

(2) *Quadratic constant stress sector.* From eqn (16) with $\sigma_{ge} = \sigma_0$, the yield criterion based on the quadratic yield criterion under plane strain conditions can be written as

$$\left[\frac{3}{4}A\left(\frac{9A+4B}{9A+B}\right)(\sigma_{rr}^2+\sigma_{\theta\theta}^2)-\frac{3}{2}A\left(\frac{9A-2B}{9A+B}\right)\sigma_{rr}\sigma_{\theta\theta}+3A\sigma_{r\theta}^2\right]^{1/2}=\sigma_0. \tag{A9}$$

The stresses should satisfy the above yield criterion.

A.2. Parabolic yield criterion

Here we examine the solutions based on the parabolic yield criterion. The parabolic yield criterion is

$$\psi(\sigma_{ij})=\sigma_e^2+c\sigma_m=\sigma_0'^2 \tag{A10}$$

where c and σ_0' are two material constants which can be expressed in terms of the uniaxial tensile and compressive yield stresses, σ_t and σ_c, as

$$c=3(\sigma_c-\sigma_t),\quad \sigma_0'^2=\sigma_c\sigma_t. \tag{A11}$$

The components of the outward normal to the yield surface are

$$P_{ij}=\frac{\partial\psi}{\partial\sigma_{ij}}=3s_{ij}+(\sigma_c-\sigma_t)\,\delta_{ij}. \tag{A12}$$

The condition $P_{33}=0$ gives

$$\sigma_{33}=\frac{\sigma_{rr}+\sigma_{\theta\theta}}{2}-\frac{\sigma_c-\sigma_t}{2}. \tag{A13}$$

(1) *Parabolic centered fan sector.* The condition $P_{rr}=0$ leads to

$$\sigma_{rr}=\frac{\sigma_{33}+\sigma_{\theta\theta}}{2}-\frac{\sigma_c-\sigma_t}{2}. \tag{A14}$$

Combining eqns (A13) and (A14) gives

$$\sigma_{rr}=\sigma_{33}. \tag{A15}$$

Combining eqns (A15) and (A13) gives

$$\sigma_{rr}-\sigma_{\theta\theta}=-(\sigma_c-\sigma_r). \tag{A16}$$

The equilibrium condition and eqn (A16) give us

$$\frac{\partial\sigma_{r\theta}}{\partial\theta}=\sigma_c-\sigma_t. \tag{A17}$$

Now we can derive the solutions for centered fan sectors as

$$\sigma_{r\theta}=\sigma_{r\theta}^0+(\sigma_c-\sigma_t)(\theta-\theta_0) \tag{A18}$$

$$\sigma_{rr}=\frac{\sigma_c\sigma_t-3\sigma_{r\theta}^2}{3(\sigma_c-\sigma_t)}-\frac{3}{4}(\sigma_c-\sigma_t) \tag{A19}$$

$$\sigma_{\theta\theta}=\frac{\sigma_c\sigma_t-3\sigma_{r\theta}^2}{3(\sigma_c-\sigma_t)}+\frac{1}{4}(\sigma_c-\sigma_t) \tag{A20}$$

$$\sigma_{33}=\sigma_{rr} \tag{A21}$$

where $\sigma_{r\theta}^0$ and θ_0 are constants.

(2) *Parabolic constant stress sector.* The stresses in the constant stress sector have to satisfy the yield criterion

$$\tfrac{3}{4}(\sigma_{rr}-\sigma_{\theta\theta})^2+3\sigma_{r\theta}^2+\frac{3(\sigma_c-\sigma_t)}{2}(\sigma_{rr}+\sigma_{\theta\theta})=\sigma_c\sigma_t. \tag{A22}$$